Cosmic rays and relations to Space Weather

Karel Kudela

IEP SAS Košice

ISWI school, Tatranská Lomnica, August 25, 2011

1. Cosmic Rays (CR).
    1.1. From history.
    1.2. CR, basic characteristics and heliosphere.
    1.3. Energetic particles (EP), CR and magnetosphere.
2. Effects of CR, EP in Space Weather (SpW) events.
3. Indirect relations of CR to SpW studies.

1. CR.
1.1 From history.

1912

Victor Hess, U. Wien – balloons to 5.3 km. Ionisation increased with altitude – cosmic rays (CR) – coming from outer space .

In **1936**, V. Hess – Nobel prize.

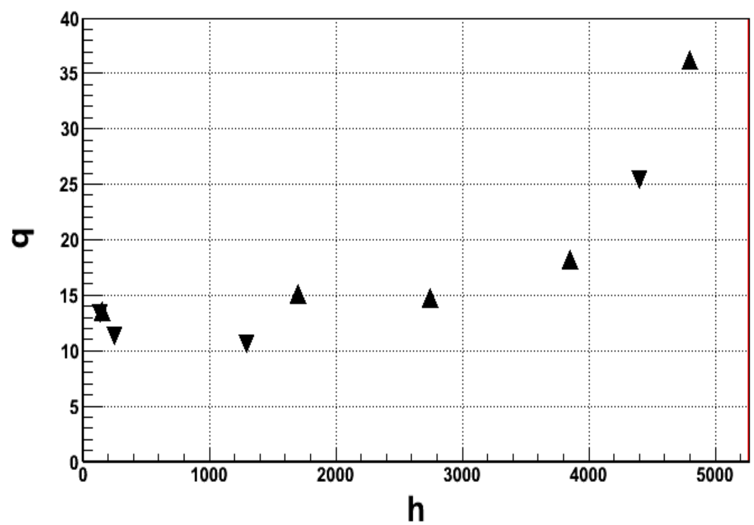

From CR history 1

- **1912**
- CR discovery - balloon.
- **1929**
- Using Cloud Chamber (particle detection by tracks) Dimitry Skobelzyn ***observed for the first time tracks of particles „induced“ from outer space***.
- **1932**
- ***Discussion about nature of this „radiation“.*** Robert Millikan – gamma rays from space, thus „cosmic rays “ is appropriate name.
- Later – not exact. ***Mainly - positively charged particles with extreme energy. CR remained as name...***
- **1933**
- ***During observations of CR in cloud chamber*** Carl Anderson discovered „anti-electron“, ***positron***. Mass of e, charge positive.

Mountains, balloons, different places on Earth / physicists studied extremely high energy CR, its nature, new particles.
At extremal energies it continues

From CR history 2

- **1937**
- Seth Neddermeyer a Carl Anderson discovered new elementary particles – ***muons in CR.***
- New scientific discipline – ***elementary particle physics*** – started due to CR research. Particle physicists used CR for study almost exclusively before 1950 (first accelerators).
- **1938**
- Pierre Auger put several detectors in Alps. He found that ***two detectors separated*** (by tens of meters or more) ***observe signals from accessing particles in time coincidence.*** Discovery ***of Extensive Air Showers*** (EAS), i.e. secondary subatomic particles created due to interactions of primaries with nuclei in air. EAS are initiated by ***primary CR with energy up to*** 10^{15} ***eV*** — by 7 orders of energy higher than those observed before.
- **1949**
- Enrico Fermi put basis to ***clarification of CR acceleration to extremal energies. One of the theories – acceleration by shock wave.*** Magnetic inhomogenities – mutual approaching. CR acceleration remains one of the fundamental questions of CR physics until now.

Hillas, 1982

TABLE 3.2. THE DISCOVERY OF THE ELEMENTARY PARTICLES

This table, an expansion of one given by Powell, Fowler and Perkins (1959), shows how and when the relatively stable elementary particles were discovered (antiparticles being included somewhat arbitrarily). The heavy lines show the discoveries made using cosmic rays. The particles are listed in order of increasing mass, except within charge multiplets.

ate
900
. .
930
931
932
933
934
935
936
937
938
939
940
941
942
943
944
945
946
947
948
949
1950

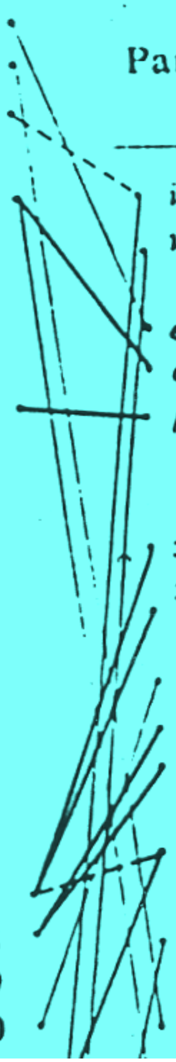

Particle		Source of radiation	Instrument used	Specific observation made
$\bar{\nu}_e(\nu_e)$		nuclear reactor	liquid scintillator	Capture by proton
ν_μ		accelerator	spark chamber	Production of μ and not e
e^-		discharge tube	fluorescent screen	Ratio e/m
e^+	●	cosmic rays	cloud chamber	Charge, mass
μ^+, μ^-	●	cosmic rays	cloud chamber	Absence of radiation loss in Pb; decay at rest; mass
π^+	●	cosmic rays	nuclear emulsion	$\pi - \mu$ decay at rest
π^-	●	cosmic rays	nuclear emulsion	Nuclear interaction at rest
π^0		accelerator	counters	Decay into γ-rays
K^+	●	cosmic rays	nuclear emulsion	$K_{\pi 3}$ decay
K^-	●	cosmic rays	nuclear emulsion	Nuclear interaction at rest
K^0	●	cosmic rays	cloud chamber	Decay into $\pi^+\pi^-$ in flight
η		accelerator	bubble chamber	Total mass of decay products
p		discharge tube	spectroscopes;	Charges and masses

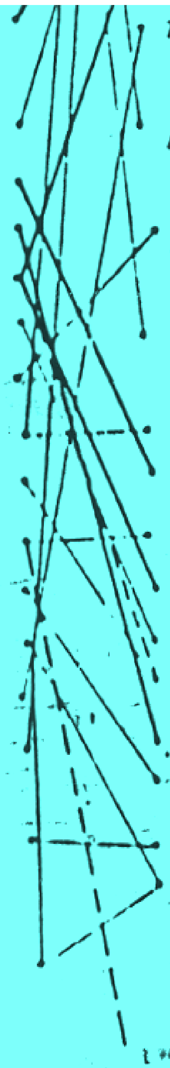

948	η	accelerator	bubble chamber	Total mass of decay products
949				
1950	p	discharge tube	spectroscopes; mass spectrometers	Charges and masses of ions
1951				
1952	$\bar{p}$	accelerator	Cerenkov counter	e/m measured; annihilation
1953				
1954	n	radioactivity	ionization chamber	Mass from elastic collisions
1955				
1956	$\bar{n}$	accelerator	counters	Annihilation
1957	Λ	● cosmic rays	cloud chamber	Decay to $p\pi^-$ in flight
958	$\bar{\Lambda}$	accelerator	nuclear emulsion	Decay to $\bar{p}\pi^+$ in flight
959	Σ^+	● cosmic rays	nuclear emulsion	Decay at rest
960	Σ^-	accelerator	diffusion chamber	Decay to $n\pi^-$ in flight
1961	Σ^0	accelerator	bubble chamber	Decay to $\Lambda\gamma$ in flight
1962	Ξ^-	● cosmic rays	cloud chamber	Decay to $\Lambda\pi^-$ in flight
1963	Ξ^0	accelerator	bubble chamber	Decay to $\Lambda\pi^0$ in flight
1964	Ω^-	accelerator	bubble chamber	Decay to $\Xi^0\pi^-$ in flight
1965	Very many "resonance" particles with			
1966	lifetimes $\sim 10^{-23}$ to 10^{-19} s			
1967		accelerator	bubble chambers	Total mass of decay products
	?"Fireballs"	cosmic rays	nuclear emulsion	Angles of meson emission
	Quarks?	not found with accelerators; being sought in cosmic rays		Charge $\frac{1}{3}$ or $\frac{2}{3}e$

1.2. Basic characteristics

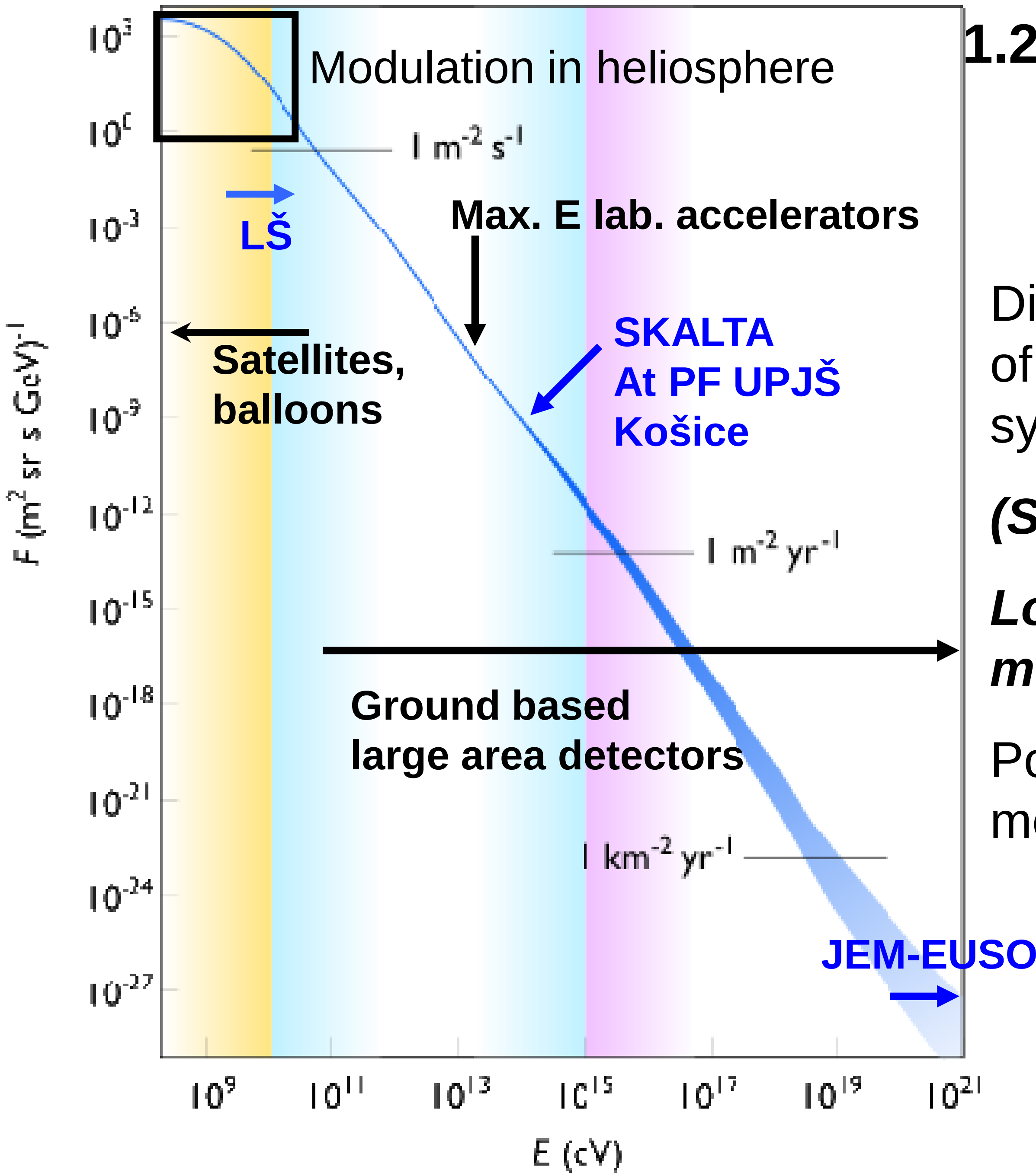

Differential energy spectrum of GCR in inner solar system.

(Simpson 1997).

***Low energy – heliospheric modulation*.**

Possibilities of measurements.

From CR history 3

- **1966**
- In 1960's, Arno Penzias a Robert Wilson found that low energy photons (microwaves, 2.725 K or 0.235 meV) fill the universe. Greisen, Kuzmin a Zatsepin – hypothesis about CR energy decrease. Interactions reduces CR energy so that ***if CR overcome intergalactic distances, its energy is below 5 x 10^{19} eV. GZK limit.***
- **1991**
- Experiment Fly's Eye in US observed primary CR with energy **3 x 10^{20} eV**. Events above **10^{20} eV** reported before.
- **1994**
- AGASA in JP reported event **2x 10^{20} eV**.
- Fly's Eye, AGASA identify highest CR energies. ***From where they come and how they are accelerated??.*** Not understood yet exactly.
- **1995**
- CR laboratory Project Pierre Auger. Gigantic fields of detectors for large amount of EAS events – aim to obtain informations about fluxes of CR with extreme energies.
- Such „tracking“ can help in understanding of origin and evolution of Universe.

***CR exceeds far the energy of accelerators*.**

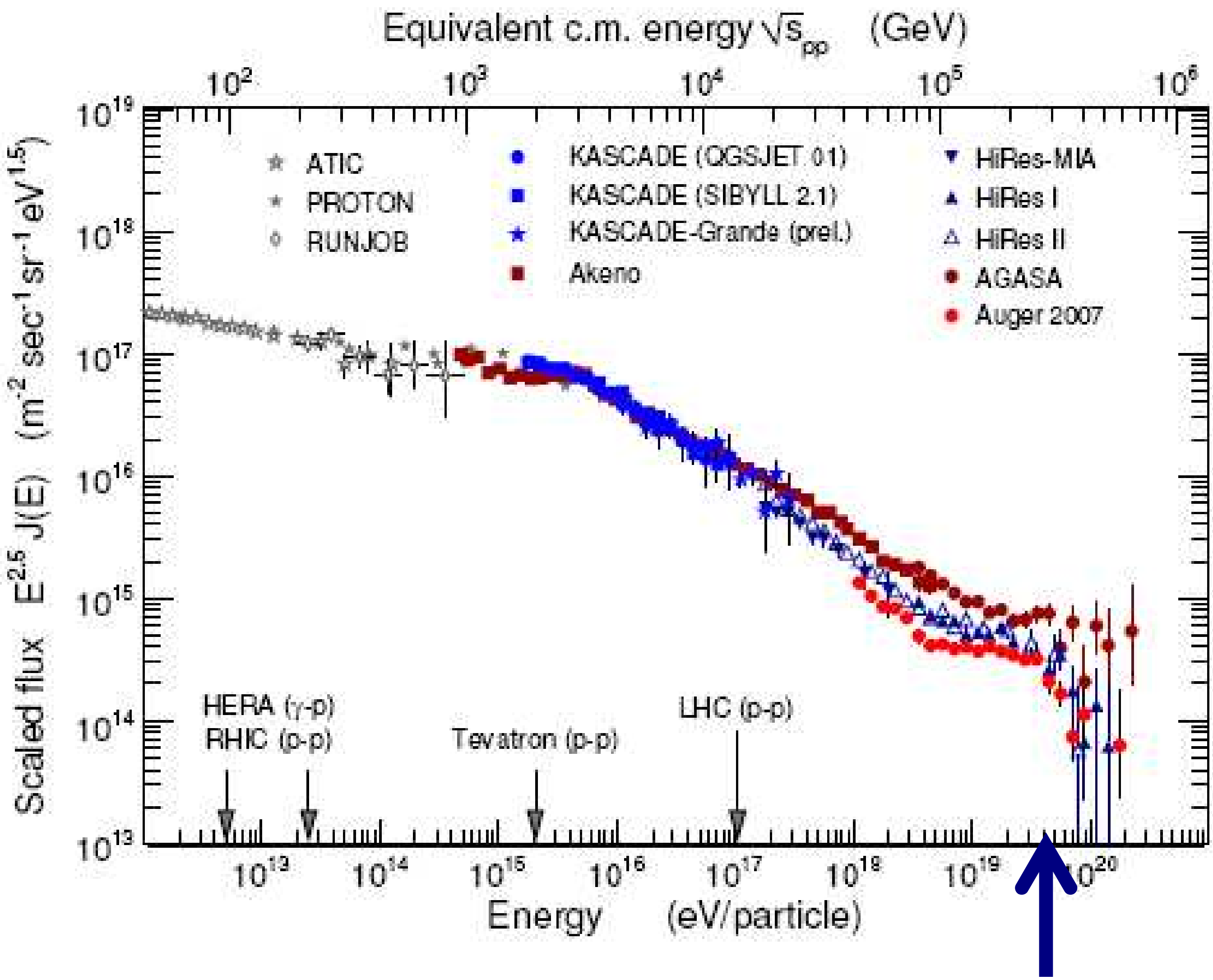

GZK effect:

CR p interact with photons CMB.

$$p + \gamma \rightarrow n + \pi^{+}$$

$$p + \gamma \rightarrow p + \pi^{0}$$

$$p + \gamma \rightarrow p + e^{+} + e^{-}$$

Extragalactic CR > 50 Mpc (163 Mly) with E > 5×10^{19} eV impossible to approach the Earth.

A. Bunyatyan, ttps://www.desy.de/~bunar/bunyatyan.eds09.HeraCr.writeup.pdf

Project JEM-EUSO.

Measurements of CR extremal energies via secondary UV radiation produced in atmosphere – looking from ISS.

Slovak version at http://jemeuso.riken.jp/JEM-EUSO_pamphlet_sk.pdf

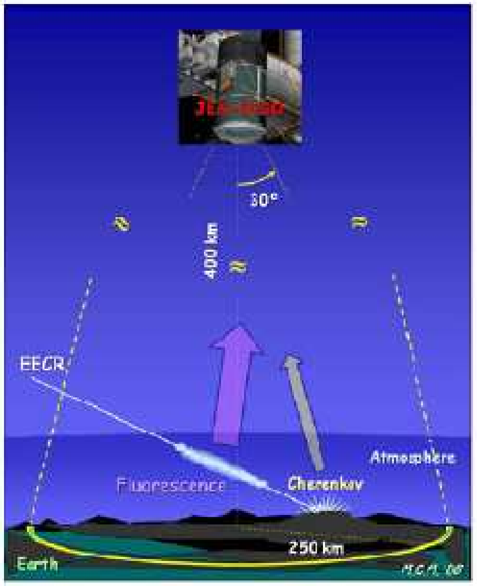

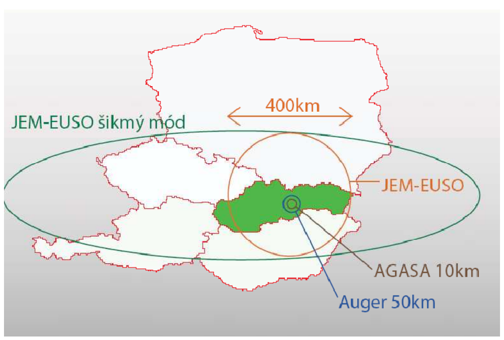

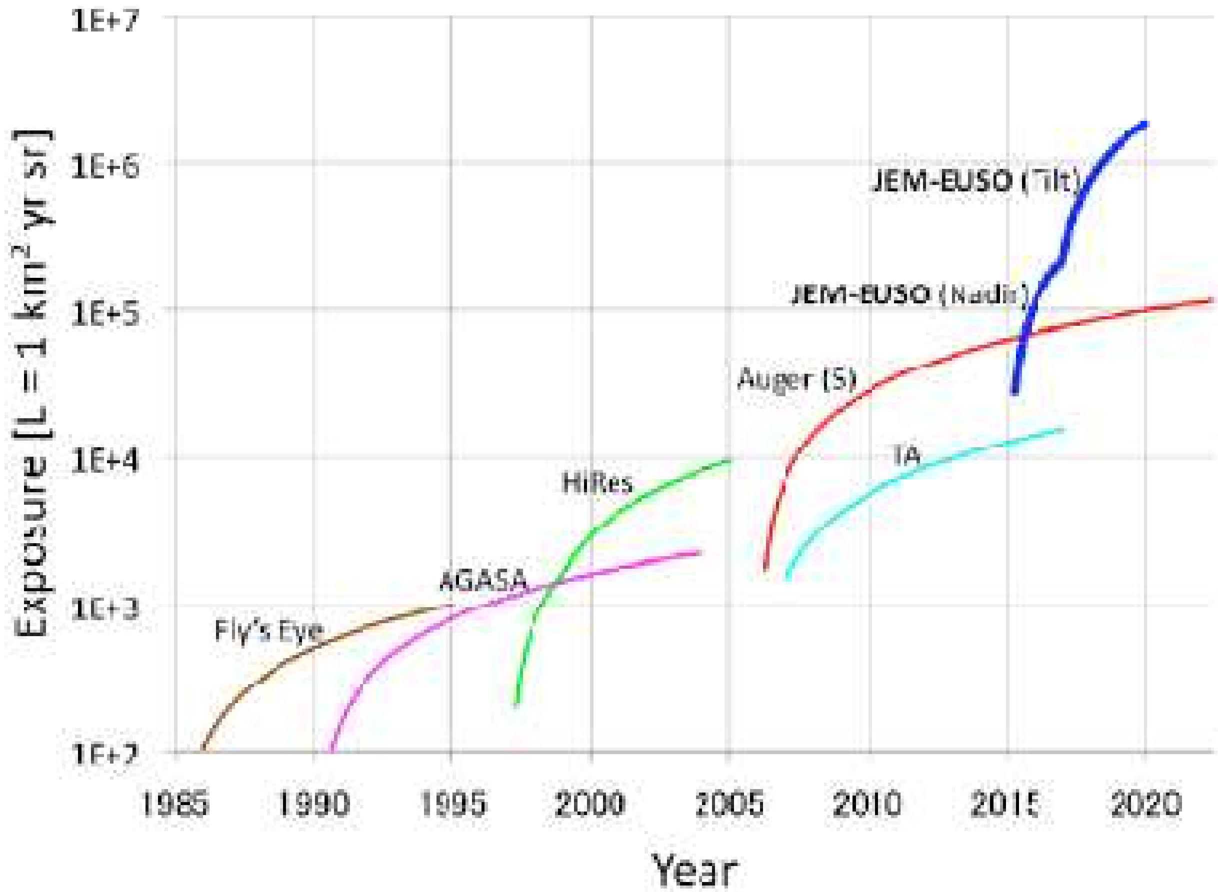

Ebisuzaki et al., 2010

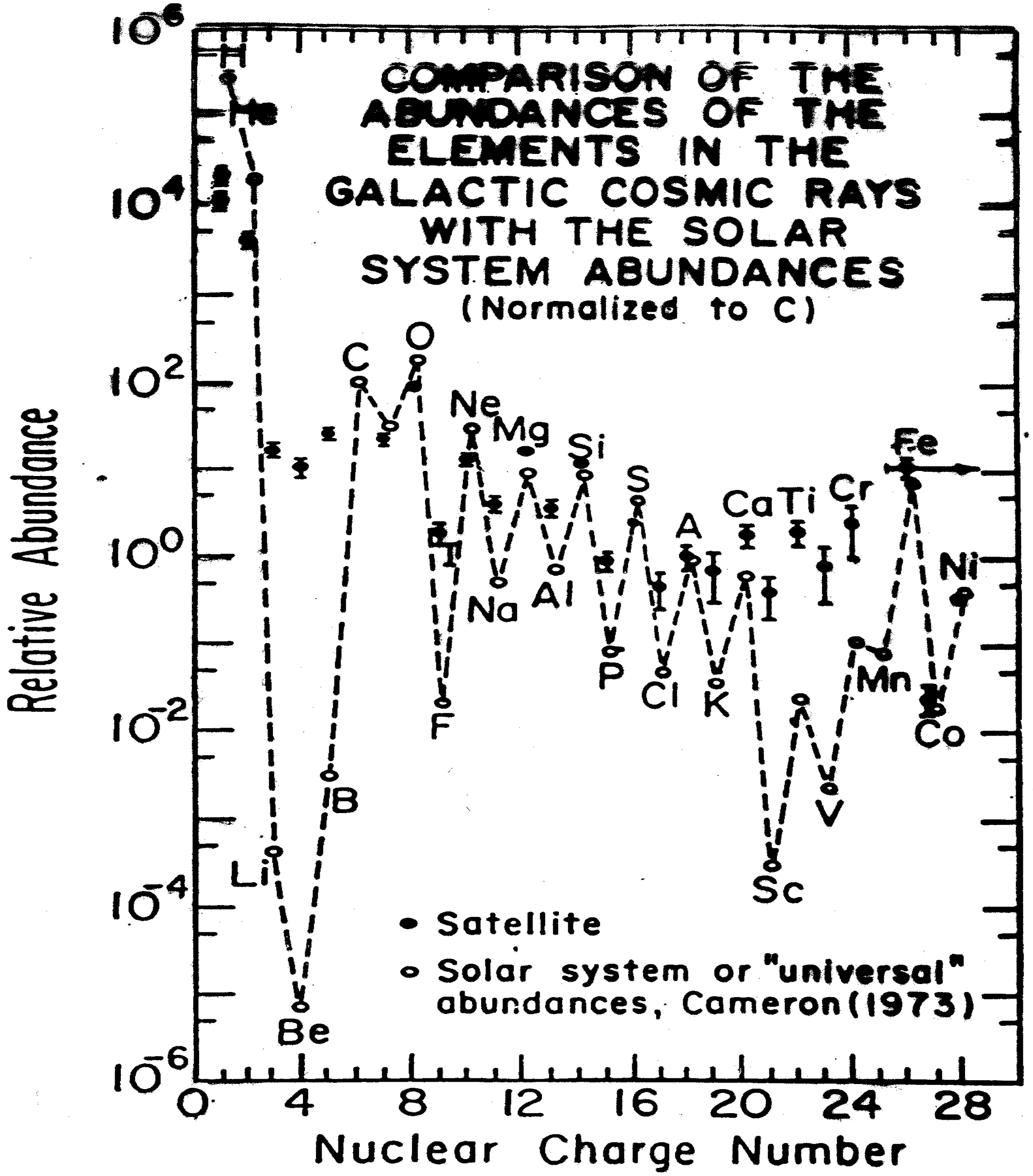

Fig. 2. Elemental composition from hydrogen to nickel in the cosmic rays arriving near the top of Earth's atmosphere. The solar system relative abundances are shown normalized to the cosmic ray carbon abundances (IMP-8 satellite).

Comparison of ***relative abundances of CR*** and ***matter of solar system*** (***Simpson, 1998***). Normalized to C (100).

Li,Be,B – fragments of heavier nuclei (C,N,O) during interactions from source to detector. Similarly Sc, V, Mn (fragments of Fe).

From chemical and isotopic composition – the total length of trajectory (depth in g/cm^2) of PRIMARY CR from source to detector.

- Although CR are rare, ***its energy density in our Galaxy (1 eV/cm^3)*** is comparable with

  energy density of light of stars

  of interstellar magnetic field

  of kinetic energy of interstellar gas (turbulence).

- Mutual interactions of CR and magnetic fields influences the evolution of galaxies

- ***CR is "second channel of information" about cosmophysical processes in addition to astronomical/astrophysical observations of photons (sensitive to the matter and fields through which passes).***

CR and heliosphere.

Voy 1 113 AU
Voy 2 92 AU
3/2010

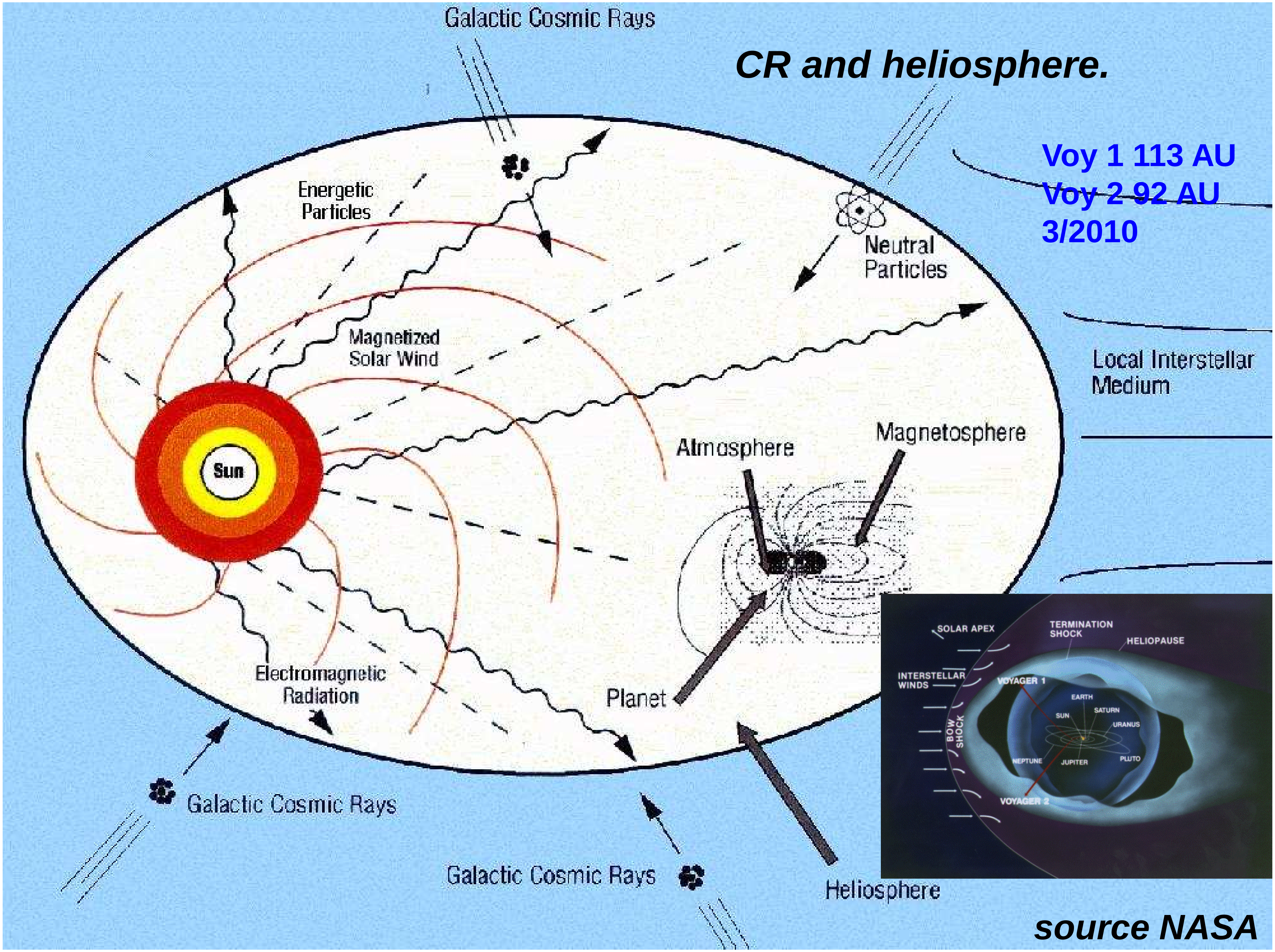

source NASA

Modulation of GCR in heliosphere – four processes in the solar wind (Parker, 1965)

CR as a response to outflow of solar wind plasma with frozen in IMF – ***convection***

CR rotate around spiral field lines and are moving along too. Inhomogenities of IMF are causing their – ***diffusion*** in pitch angle space (isotropic in reference frame of SW).

SW plasma either *expands* (outflow from solar surface) or *compresses* (shock waves) – CR is either adiabatically cooled or heated – ***adiabatic heating***

Since gyromotion around field lines is faster than diffusion (scattering), CR undergoes to ***drifts*** due to large-scale structure of „spiral“ IMF (curvature, gradient).

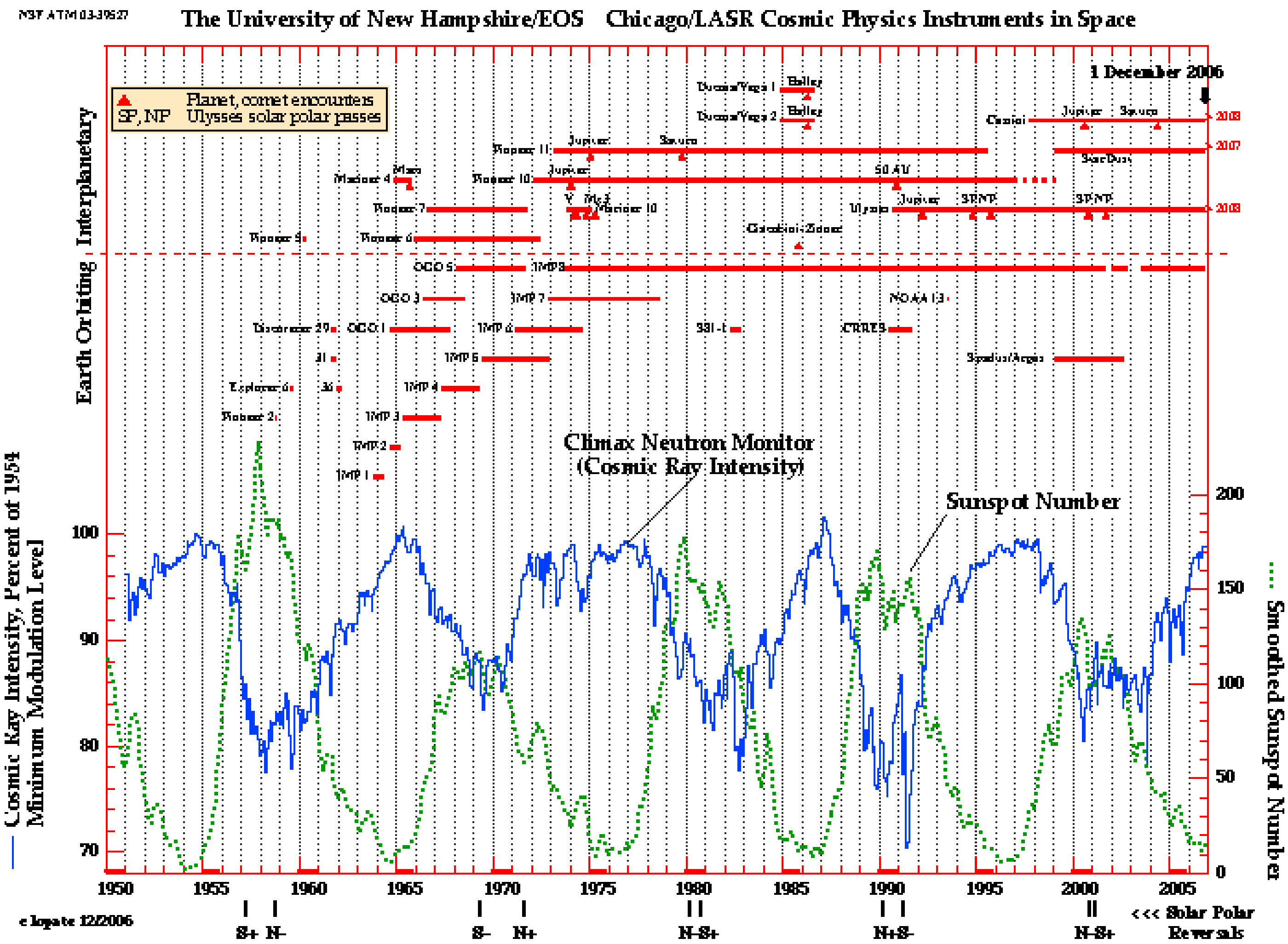

CR variability
at NM energies
- 11, 22 yr

http://ulysses.sr.unh.edu/NeutronMonitor/Misc/neutron2.html

PSD: many transitional effects with variable duration, few quasi-periodic variations.

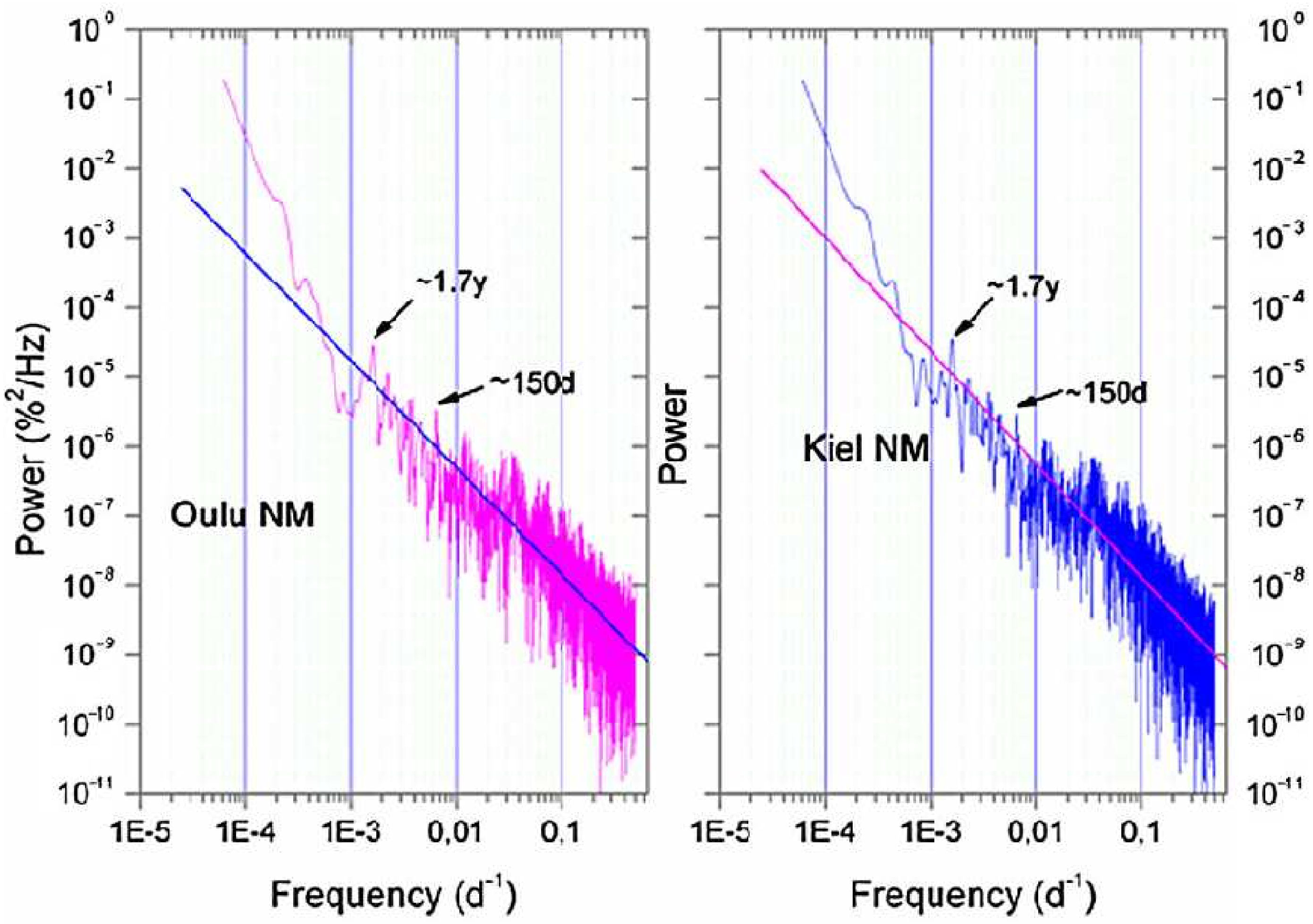

Figure 1 Power spectra of Oulu and Kiel neutron monitors constructed from daily means of pressure-corrected data for the period from day 92 of year 1964 until the end of year 2008.

Kudela et al., 2010

Irregular variations, recent example: Decrease of CR (FD) 5-7 August 2011,
Data of IMF and SW by U.S. Dept. of Commerce, NOAA, Space Weather Prediction Center

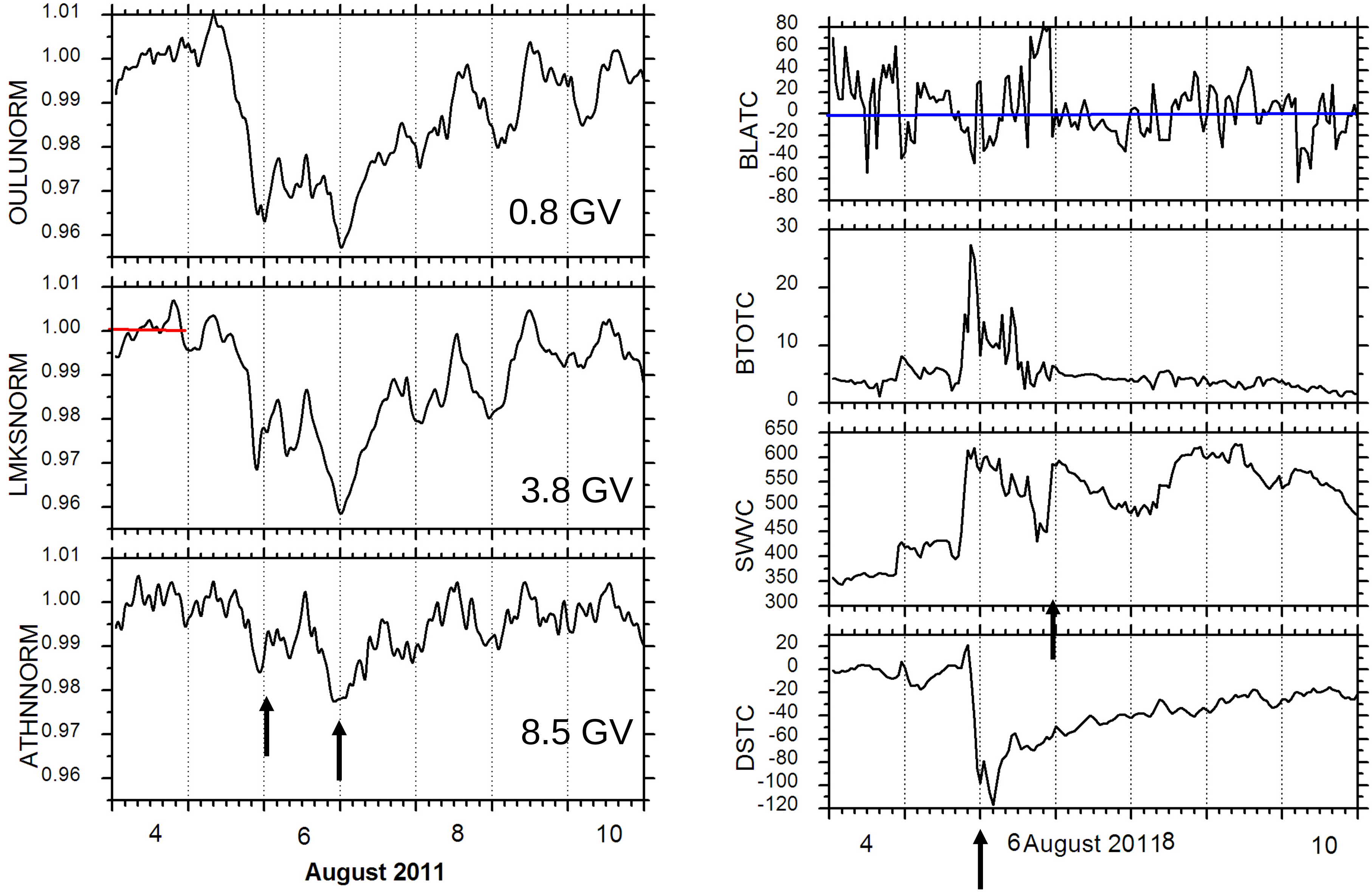

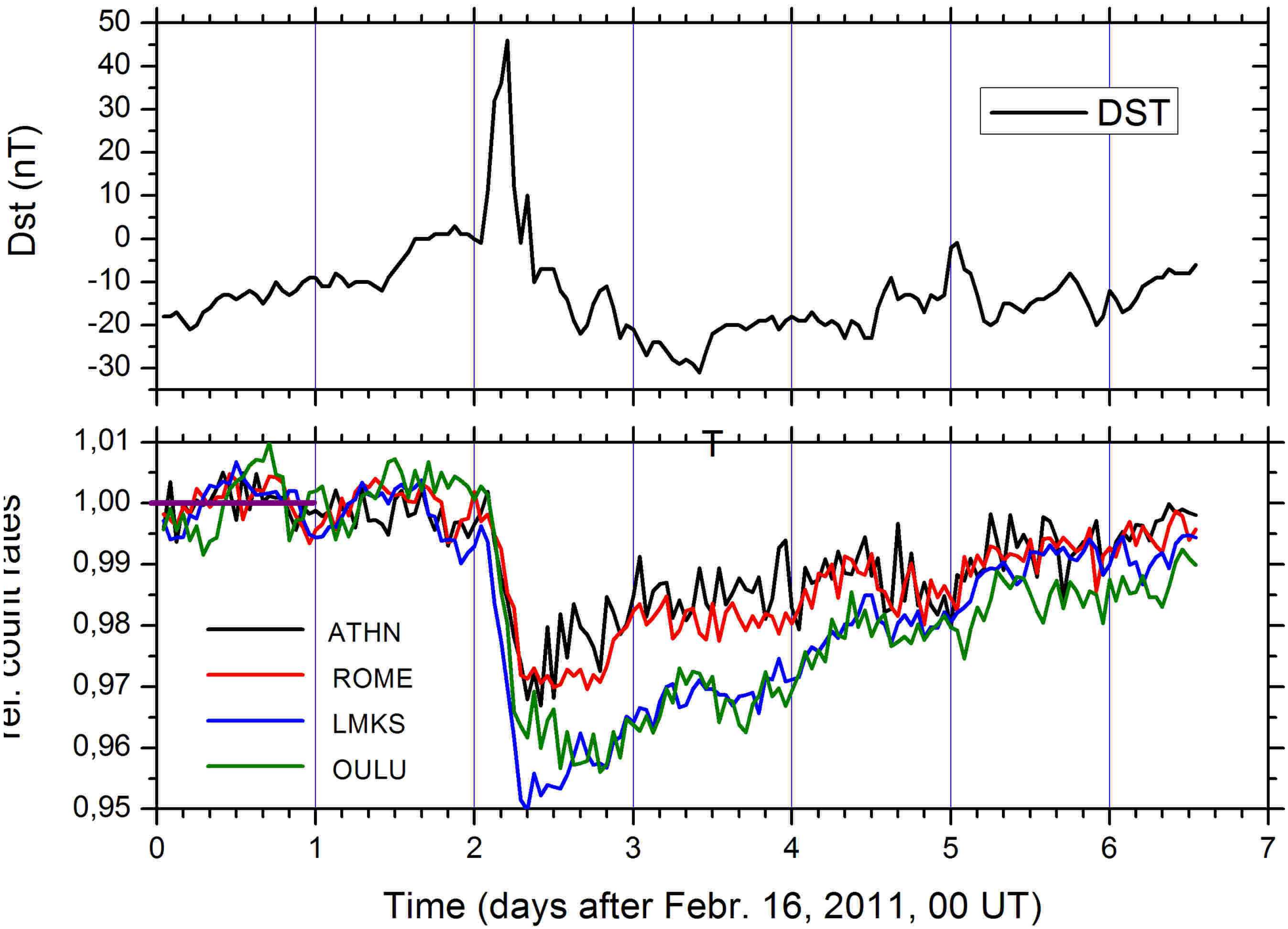

IMF Bz>0, no geomagnetic storm, FD clear

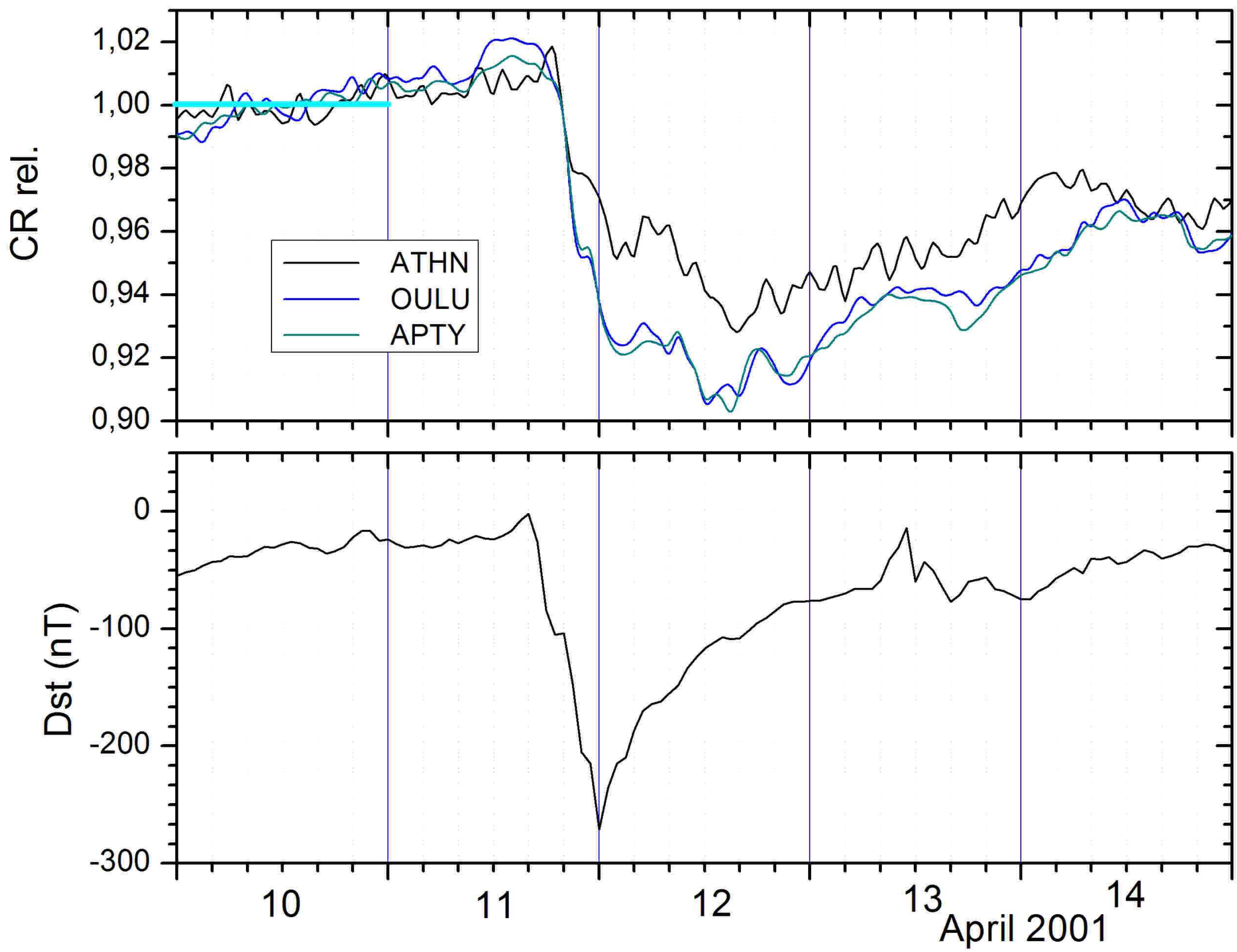

For Bz<0, geomagnetic storm, Dst depression, more usual

Short term increases – during some of solar flares GLE events.

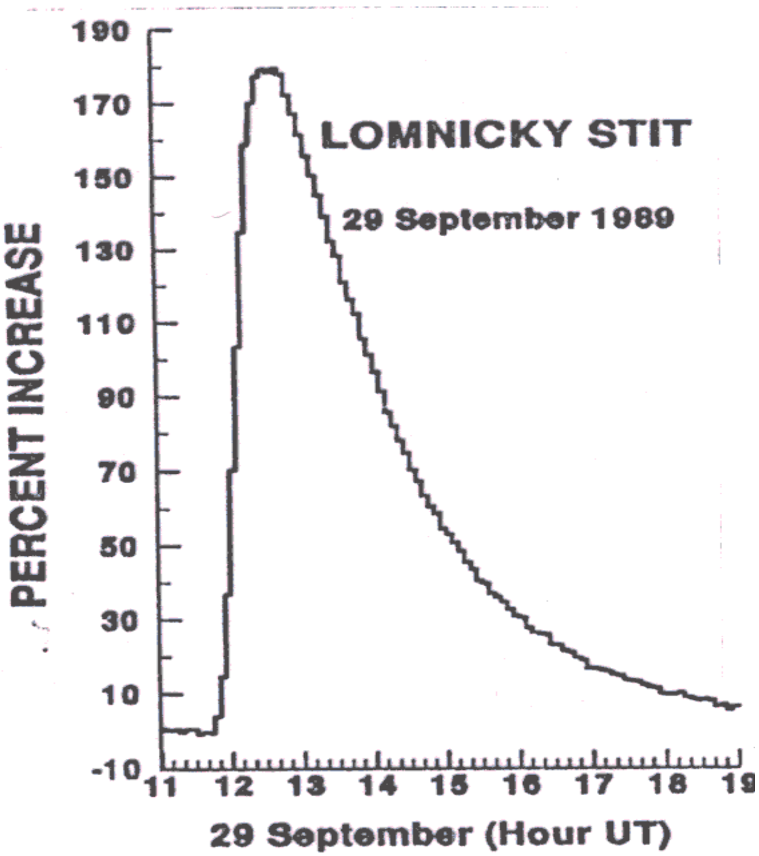

Figure 1. Cosmic ray intensity recorded at Lomnicky Stit during the GLE on 29 September 1989.

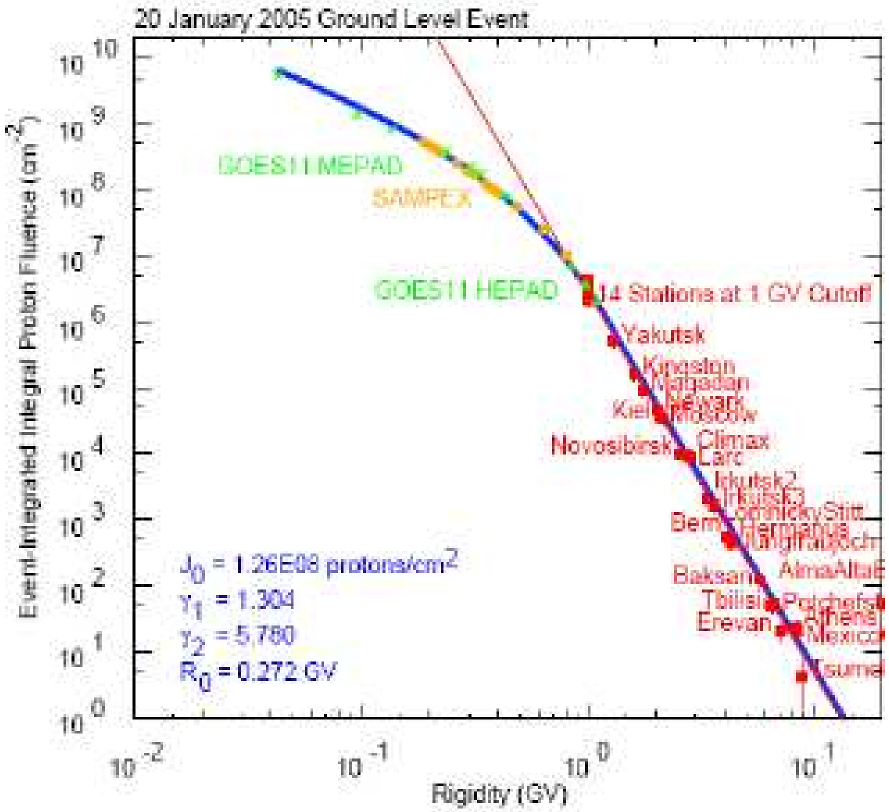

Network of NM and satellite data – combining to obtain energy spectra in wide energy range (Usoskin, Tylka, 2009)

3.6.1982 – first response from solar neutrons in flare at the ground (LŠ along with Jungfraujoch), E.L. Chupp on SMM gamma.

1.3.Energetic particles (EP), CR and magnetosphere.

Milestones

1957 MEDZINÁRODNÝ GEOFYZIKÁLNY ROK (aj v ČSR)

1958 Objav radiačných pásov Zeme — *VAN ALLEN, VERNOV*

1958 Prvé merania slnečného vetra — *GRINGAUZ*

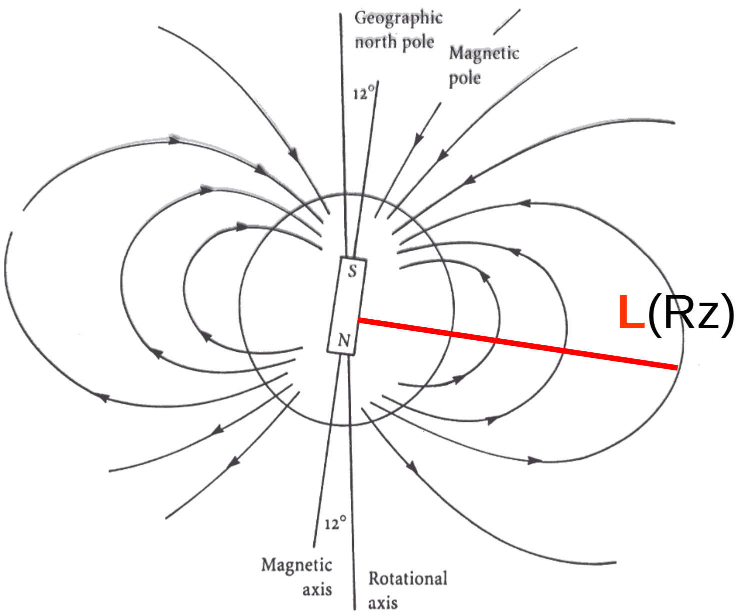

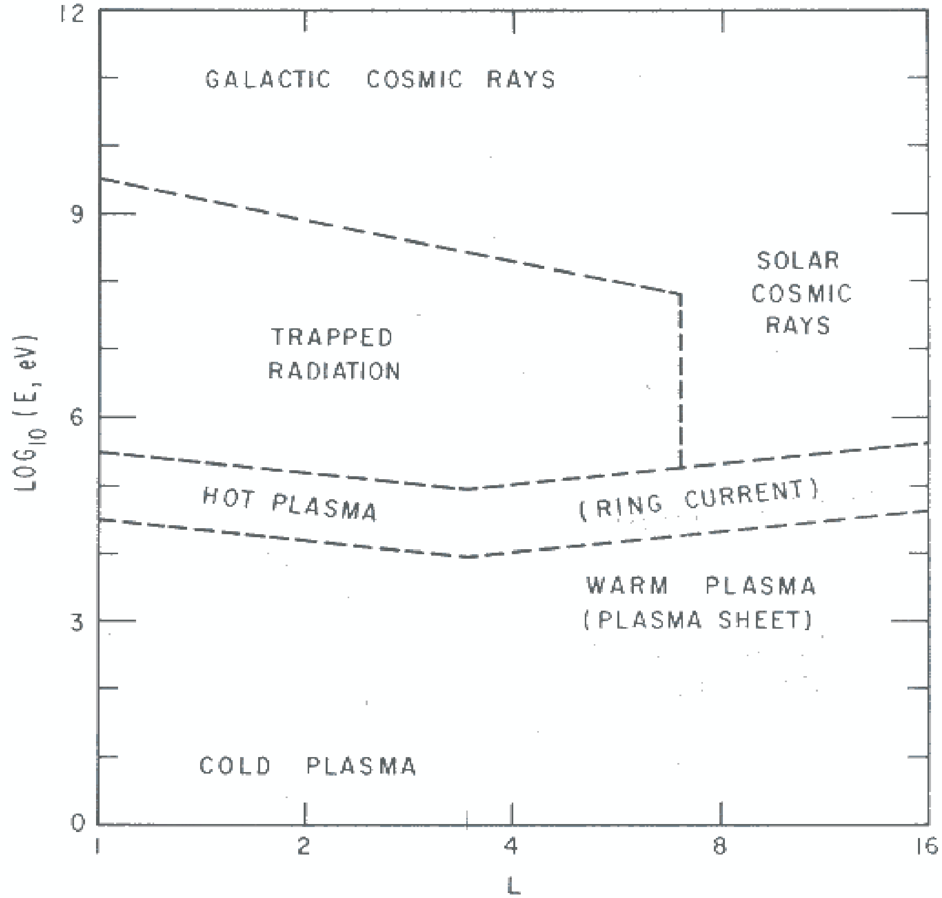

L – McIlwain, 1966

Hutchinson, Lang, Roederer

http://radbelts.gsfc.nasa.gov/outreach/Radbelts6.html

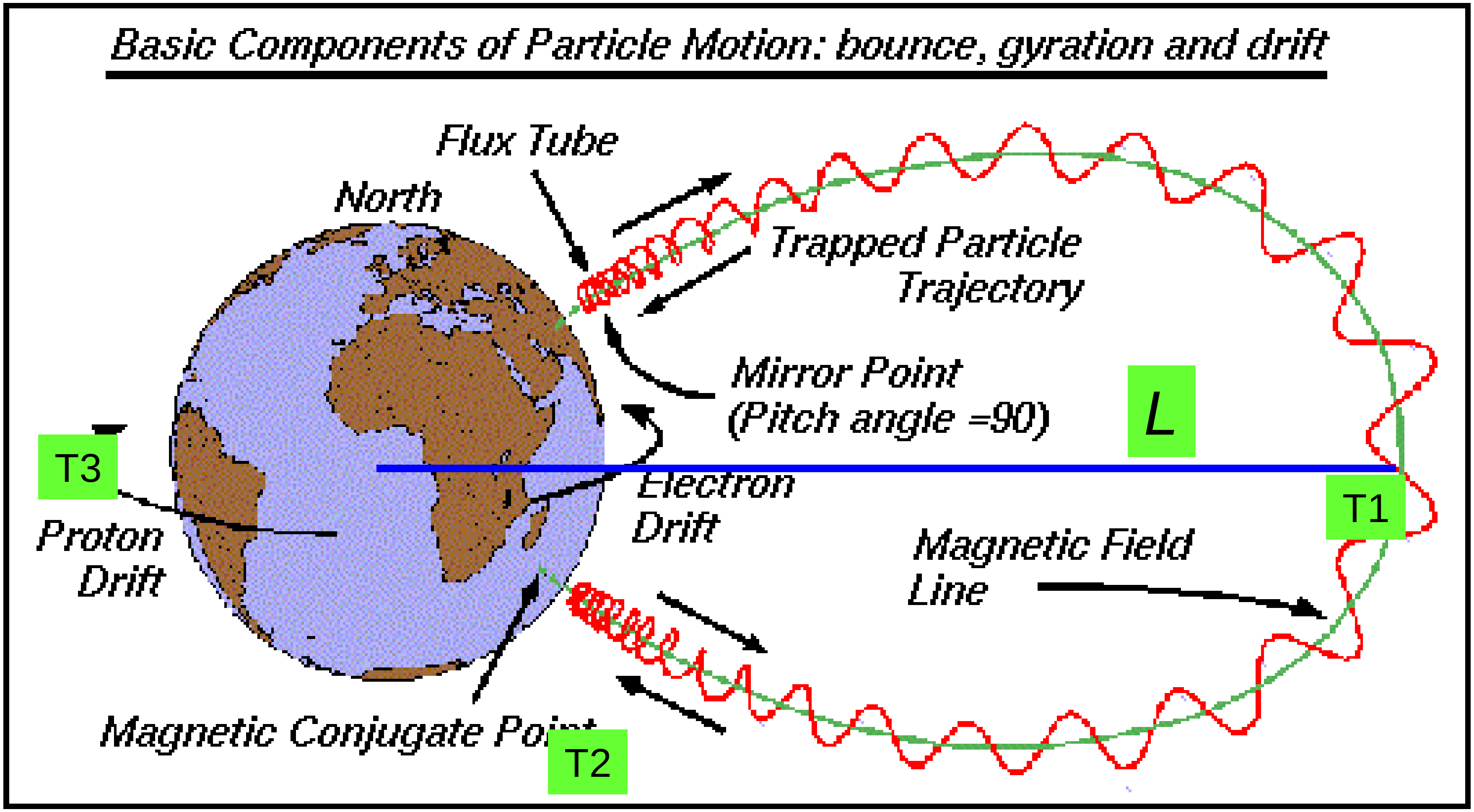

Instead of 3D – using 2D (coordinates L,B)

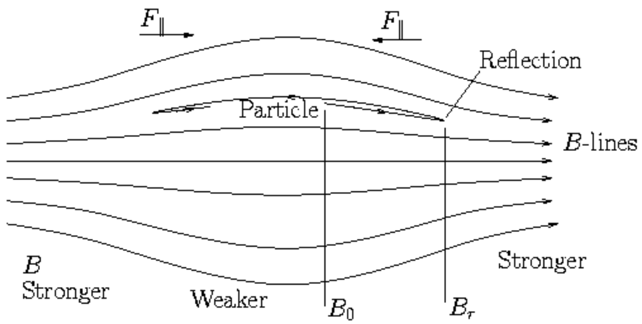

http://silas.psfc.mit.edu/introplasma

CR

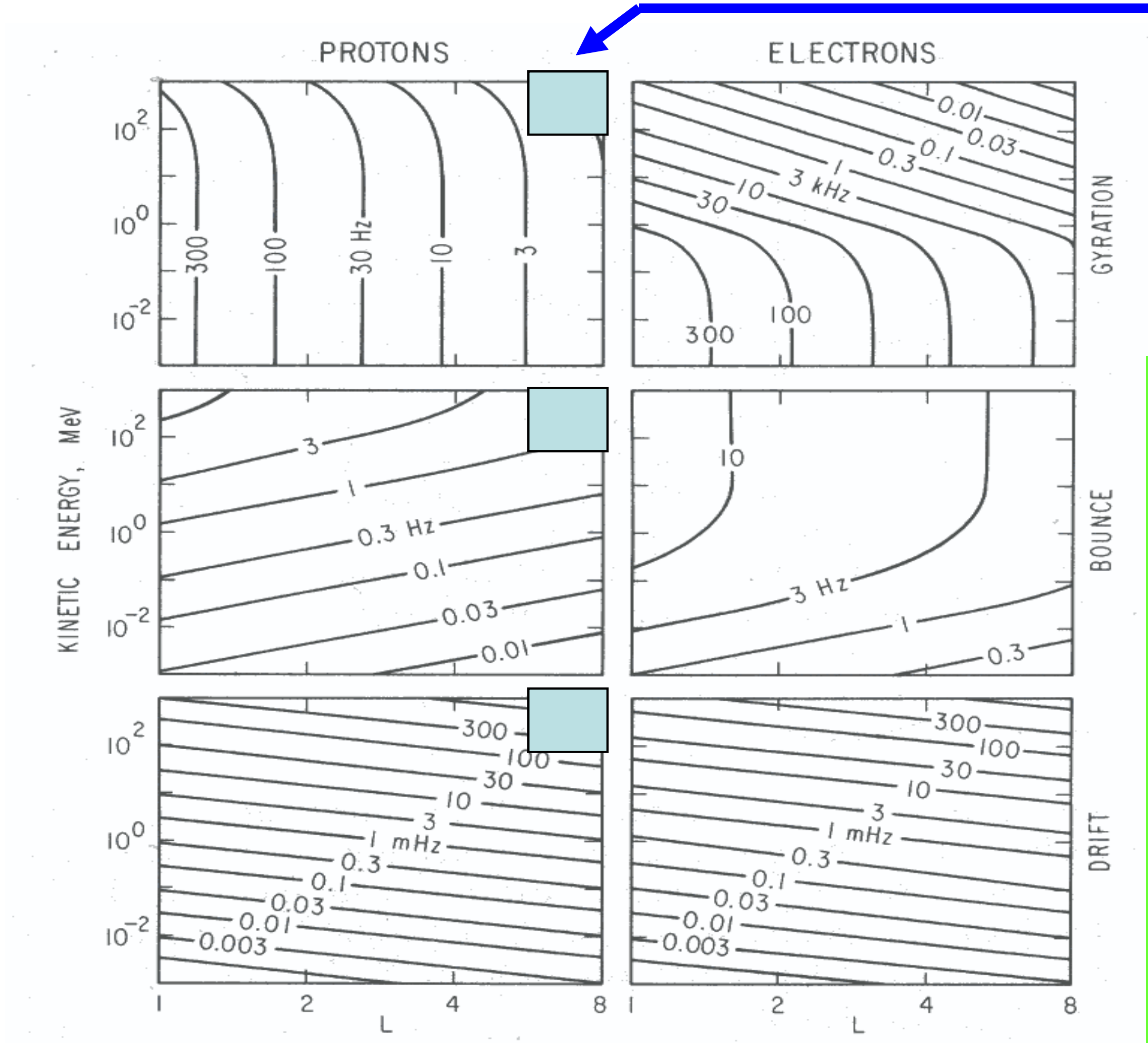

T1<<T2<<T3 (1)

If (1) – guiding center.

If not (1), **CR** – only way numerical tracing of particle trajectory in model field.

Roederer, 1970

CR – access to magnetosphere – for static field model IGRF – trajectories numerically traced, asymptotic directions.

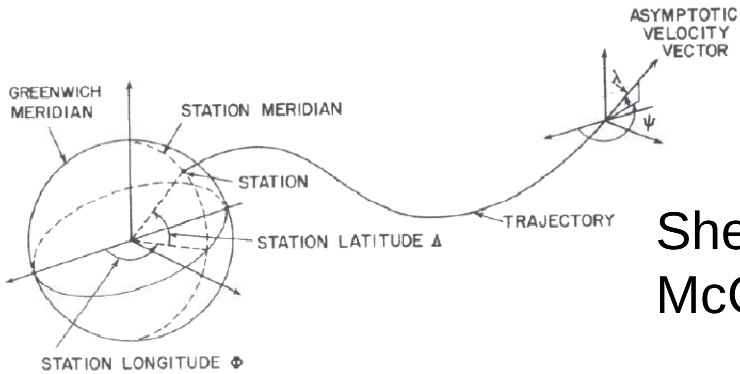

Shea, M. A., Smart, D. F., and McCracken, K. G.: 1965

During geomagnetic storm the models give different asymptotic directions and transmissivity.

Trajectory computations for LŠ - quiet, disturbed period

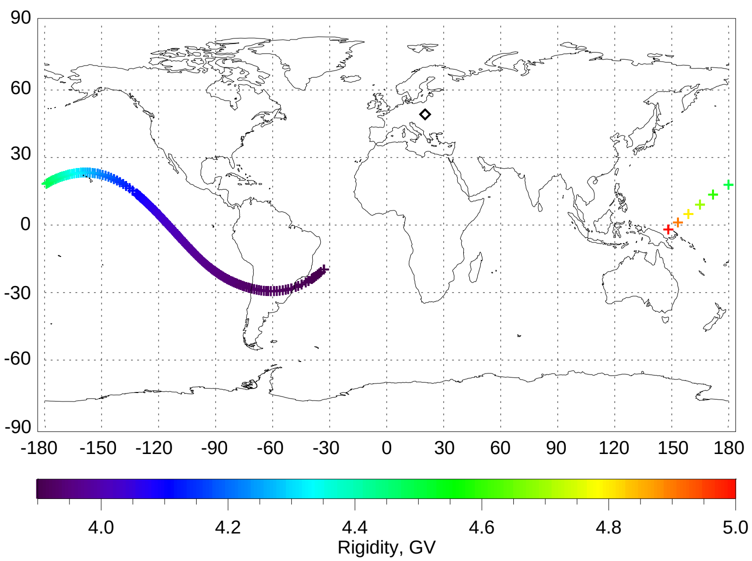

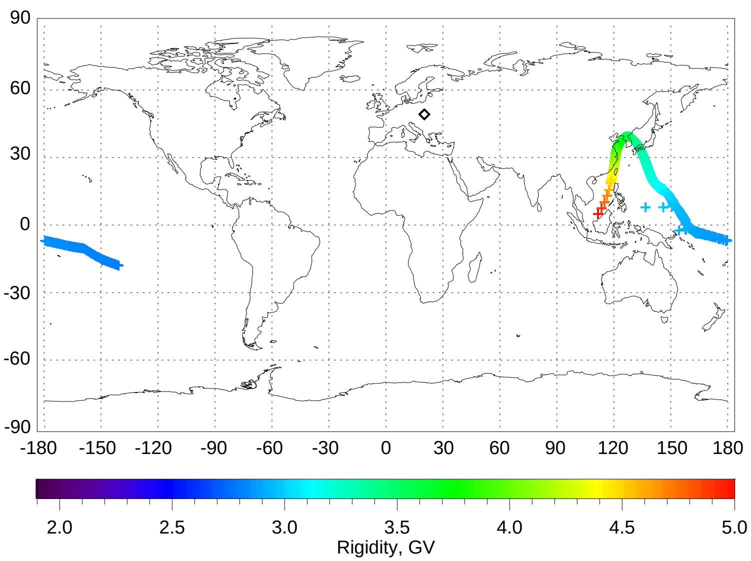

Variability of transmission of CR via magnetosphere during geomagnetic storm

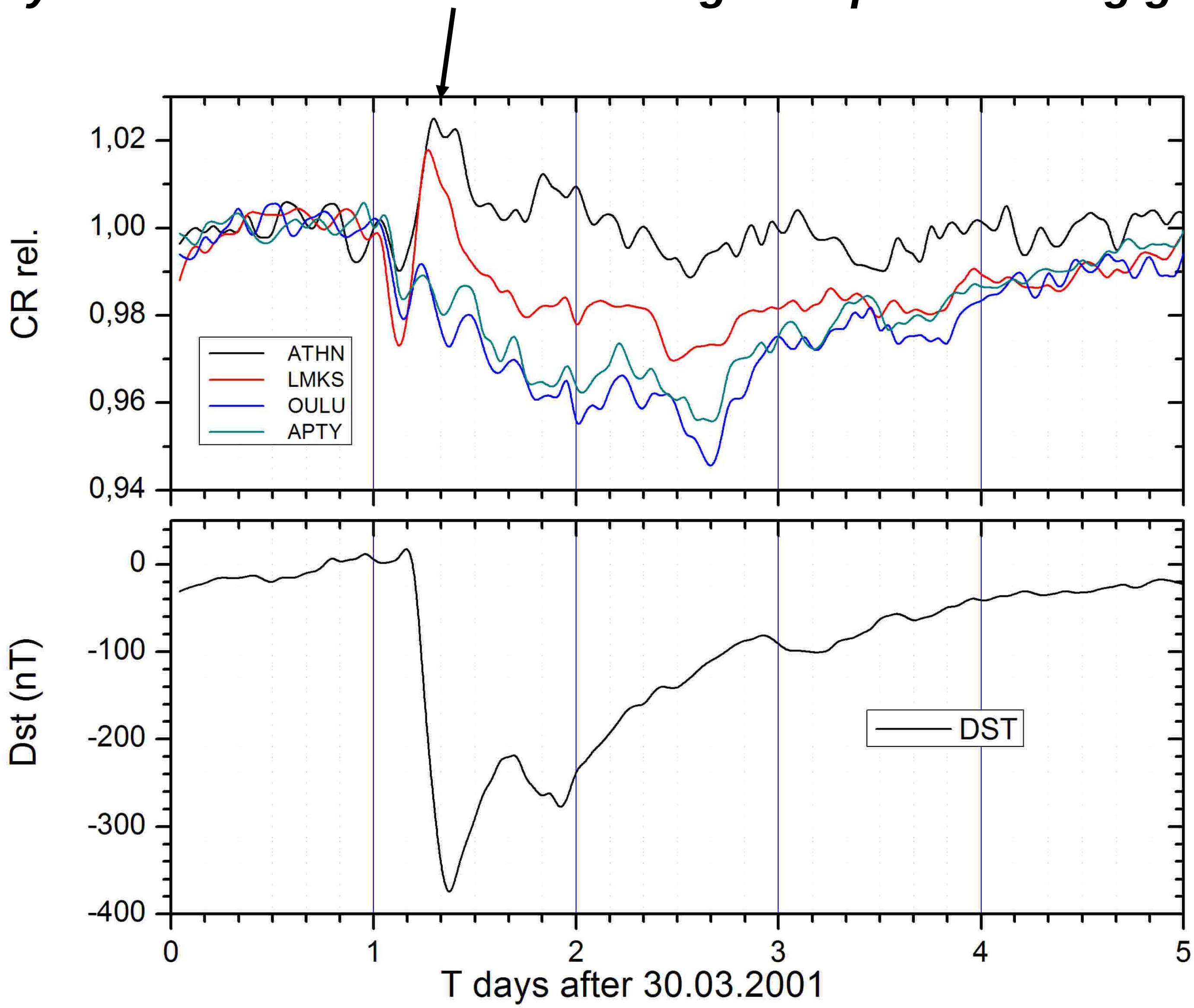

Increase of CR especially at NMs with higher cut-off (Athens for example).

Merania na

H. MORAAL ET AL. 2000

TABLE 1

Neutron monitors with the highest counting rate

Station	Lat. (deg)	Alt. (m)	Press. (mb)	Cutoff (GV)	Counting rate s^{-1}	Statist. rank
Tibet	30.1	4300	606	14.1	2970	1.00
Alma Ata B	43.3	3340	680	6.61	1205	0.64
Erevan	40.2	2000	815	7.58	1100	0.61
Haleakala	20.7	3030	700	12.9	970	0.57
Lomnický Štít	49.2	2634	748	3.98	420	0.38
Jungfraujoch 2	46.5	3475	646	4.61	330	0.33
Tsumeb	−19.2	1240	880	9.21	310	0.33
Calgary	51.1	1128	883	1.08	270	0.30
South Pole	−90.0	2820	680	0.09	260	0.29
Irkutsk 3	52.3	3000	715	3.64	240	0.28
McMurdo	−77.9	48	1007	0	230	0.28
Irkutsk 2	52.3	2000	800	3.64	210	0.26
Moscow	55.5	200	1000	2.43	200	0.26
Kerguelen	−49.4	0	1000	1.14	190	0.25
Inuvik	68.3	21	1010	0.17	160	0.24
Novosibirsk	54.8	163	1000	2.87	160	0.23

NM (8)

http://neutronmonitor.ta3.sk

7FP EU project NMDB, also Lomnický štít **, http://nmdb.eu**

2. Effects of CR, EP in Space Weather (SpW) events.

The conditions on the sun and in the solar wind, magnetosphere, ionosphere, and thermosphere that can influence the performance and reliability of space-borne and ground-based technological systems and endanger human life or health.

Energetic charged particles can cause SEU, radiation damage, degradation and change of potential of elements of space systems. At higher energies – electronics at airplanes can be influenced.

Radiation is potentially limiting factor for interplanetary missions with people.

Effects of cosmic rays on Spacecraft and Aircraft Electronics are listed e.g. in papers

(C. Dyer and D. Rodgers, ESA WPP-155, 17-26, 1999;

E.J. Daly, ESA SP-477, xvii-xxiv, 2002 among others)

Total dose effects

Lattice displacement damage

Single event upsets (memories corrupted)

Electrostatic charging, deep dielectric charging

High energy particles interacting with materials contribute to three types of processes:

ionisation or excitation of atoms/molecules
destruction of crystal structures and molecular chains
nuclear interactions (at very high energy).

Heavy (p)

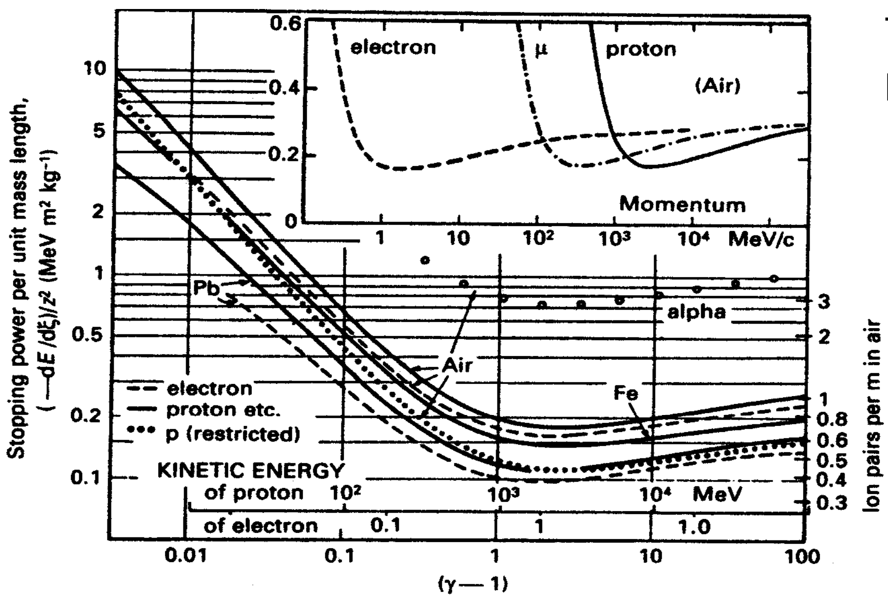

Figure 2.7. The energy loss rate due to ionisation losses in various materials. In contrast to Fig. 2.6, these curves extend into the relativistic regime, $\gamma \gg 1$. The diagram shows both the values of the Lorentz factor γ and the kinetic energies of the particles. The inset shows the loss rates in air as a function of the momentum of the particles. (From A. M. Hillas (1972). *Cosmic rays*, page 30, Oxford: Pergamon Press.)

Ranges for protons and alpha particles can be found at

http://physics.nist.gov/PhysRefData/Star/Text/programs.html

A complete ***review on particle interaction and displacement damage in silicon devices operated in radiation environment*** including (not only) effects in space was published e.g. in (*Leroy and Rancoita, Rep. Prog. Phys., 2007; 2009*).

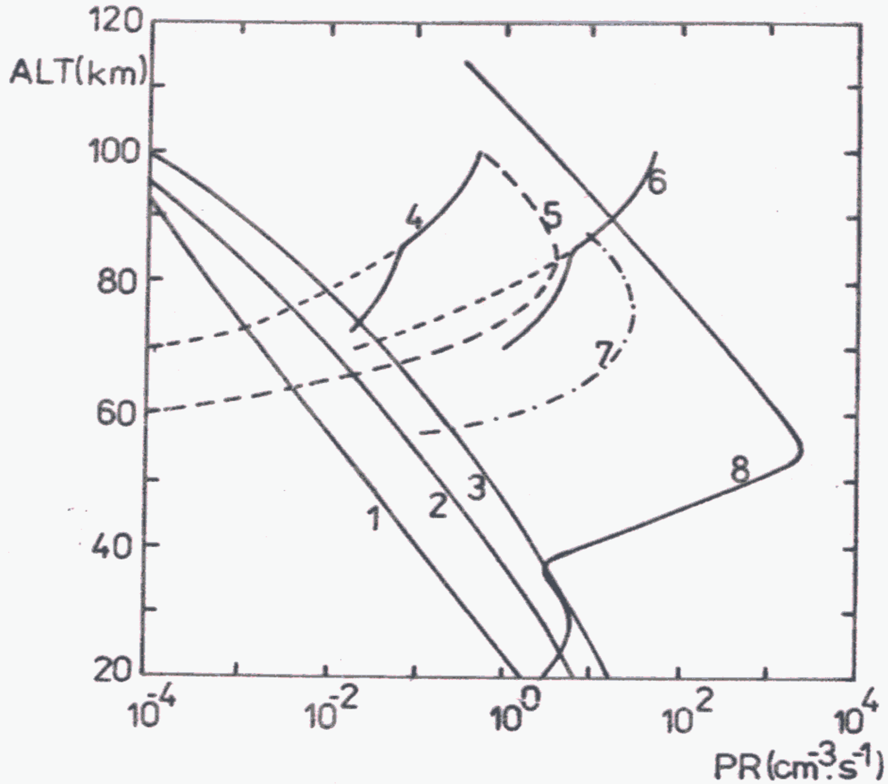

Ionisation (production rate of ions) in atmosphere at different altitudes by cosmic rays and by other energetic particles. Simplified picture.

Compilation of :
Vampola and Gorney, 1983
Baker et al, 1987
Sheldon et al, 1988

1, 2, 3 – GCR at 0°, 70° s.max, 70° ~~s.min~~ Velinov, 1974

4, 6 – solar H_α (scattered, direct)

5, 7 – due to e precipitation (quiet, $K_p = 6_-$) at $L = 4$

8 – due to relativistic electrons (assumed $L \in (3, 8)$)

At sea level only part of dose is from CR

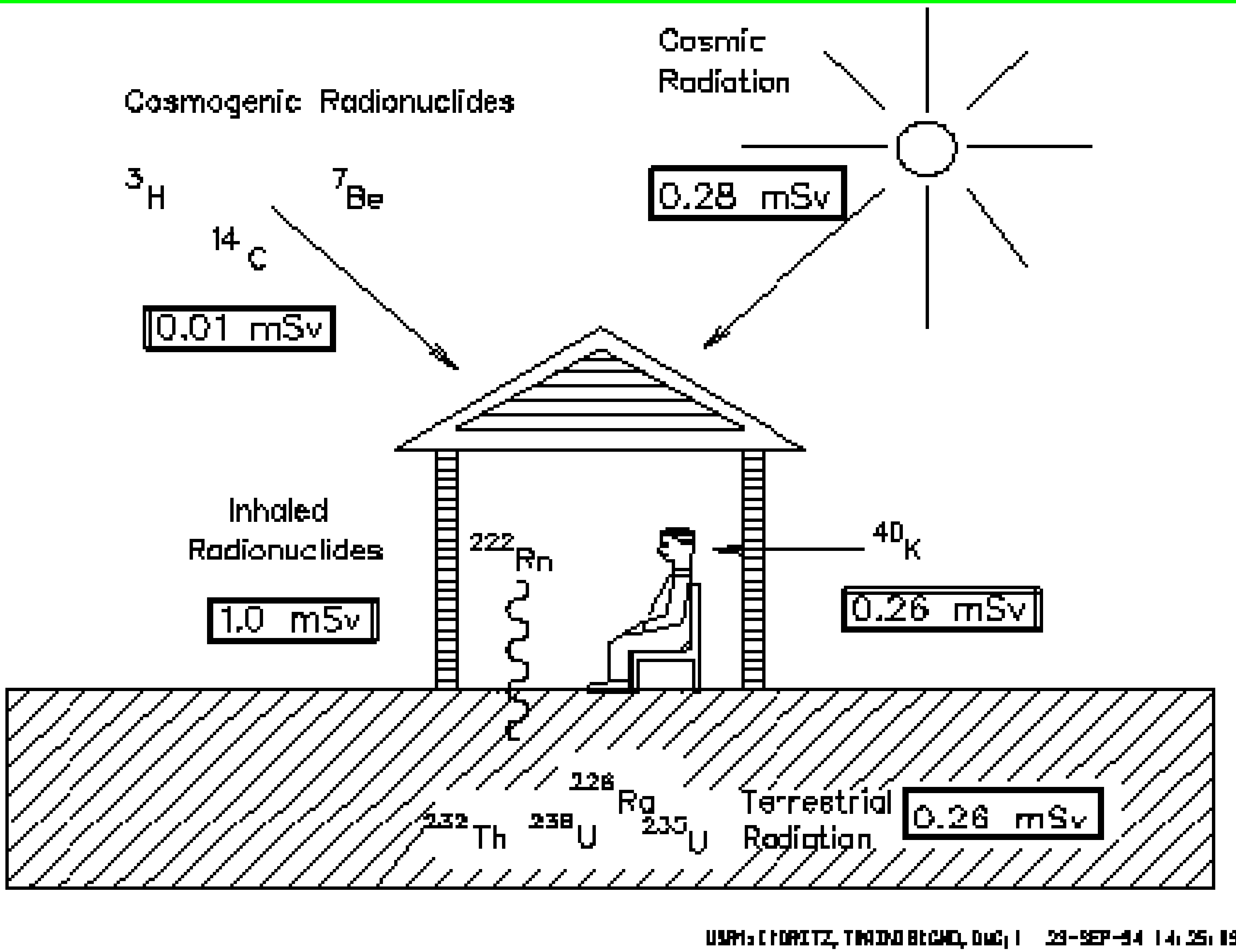

per year

Sievert (Sv) – SI unit – absorbed dose multiplied by quality factor – measure of probability that specific dose of given type of radiation cause biological effect (1J/kg)

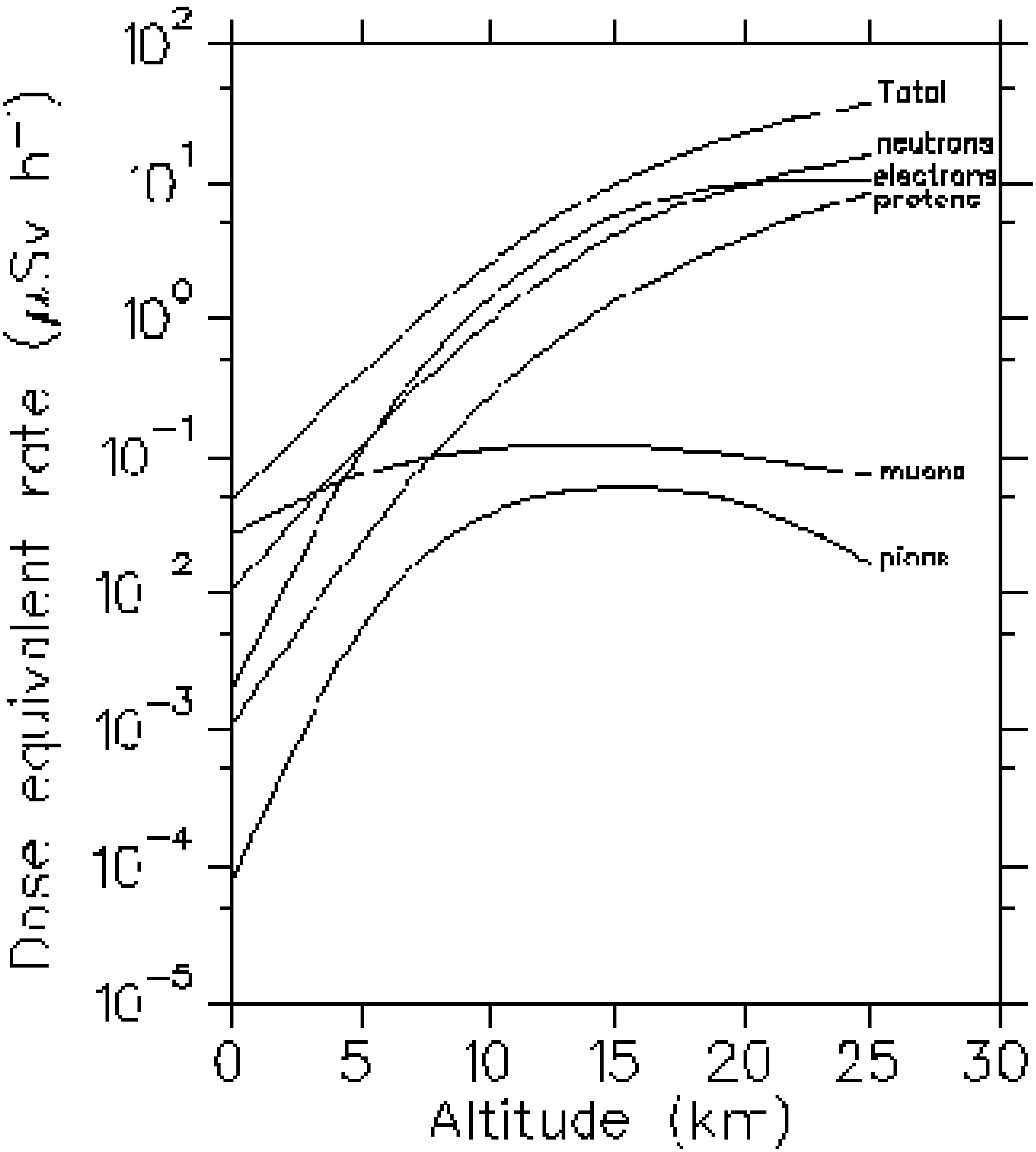

Dose increases with the altitude and relative contribution of different secondaries is changing.

Middle latitudes, only GCR

More e.g. in paper Reitz, 1993

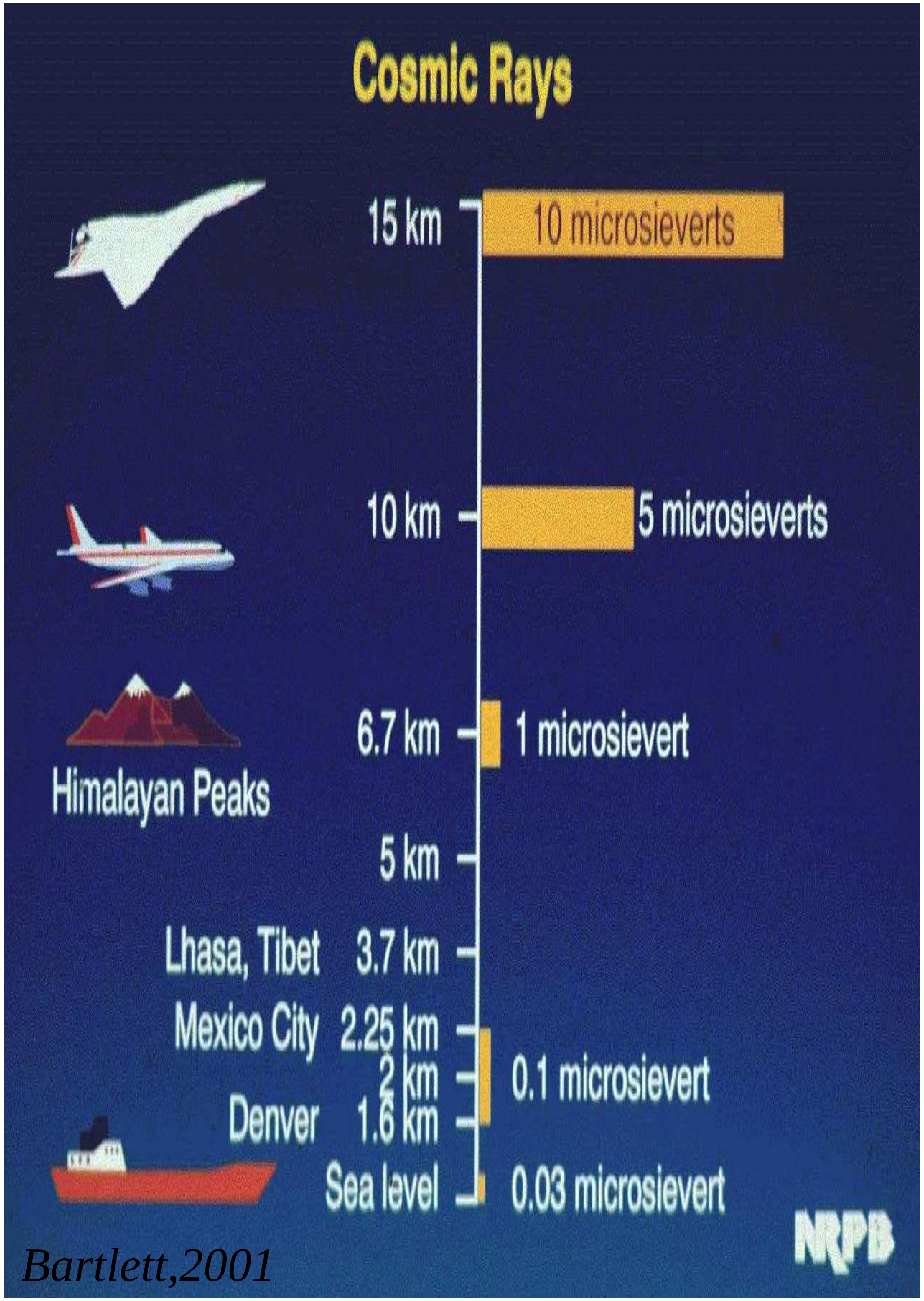

Bartlett,2001

GCR:

During 1 week ***at 10 km***, 1GV, 0.7 mSv

During strong GLE 23.2.1956 2-3x more (few hours)

During „weaker“ flare in 1989 – dose half after 2 hours

At 17 km: total dose 1.8mSv

During GLE 1956 ~ 9.3mSv (1SEU every 7 s!)

(for astronauts in free space - probably fatal consequences)

Dyer, 2001)

COSMIC RAY IMPLICATIONS FOR HUMAN HEALTH

TABLE I

Variation in cosmic ray exposure

Effect	Range of variation	Within Magnetosphere
Altitude	Factor of 1000	From sea level to 80 000 ft
Latitude	Factor of ~2	Highest at polar latitudes
Solar cycle	Factor of ~2	Highest at high latitude
Solar protons	Variable	Highest at polar latitudes; short lived transient events

Shea, M.A. and Smart, D.F., 2000

Solar CR significantly changes the dose at airplane altitudes.

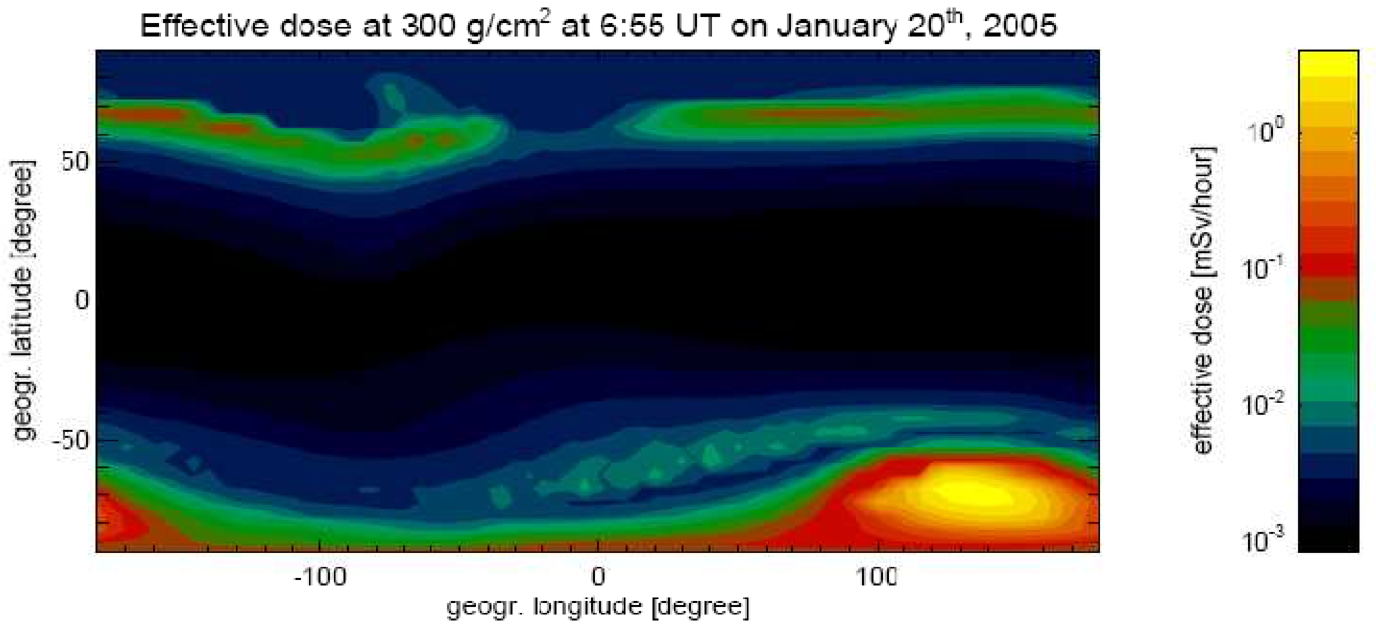

Results of the computations of the dose done by using the code PLANETOCOSMICS http://cosray.unibe.ch/~laurent/planetocosmics/ (group of University of Bern, Switzerland) for January 20, 2005 event.

Dose is increasing during solar flare/CME acceleration of protons to high energy. From (*Spurný, F. and Dachev Ts., 2001*).

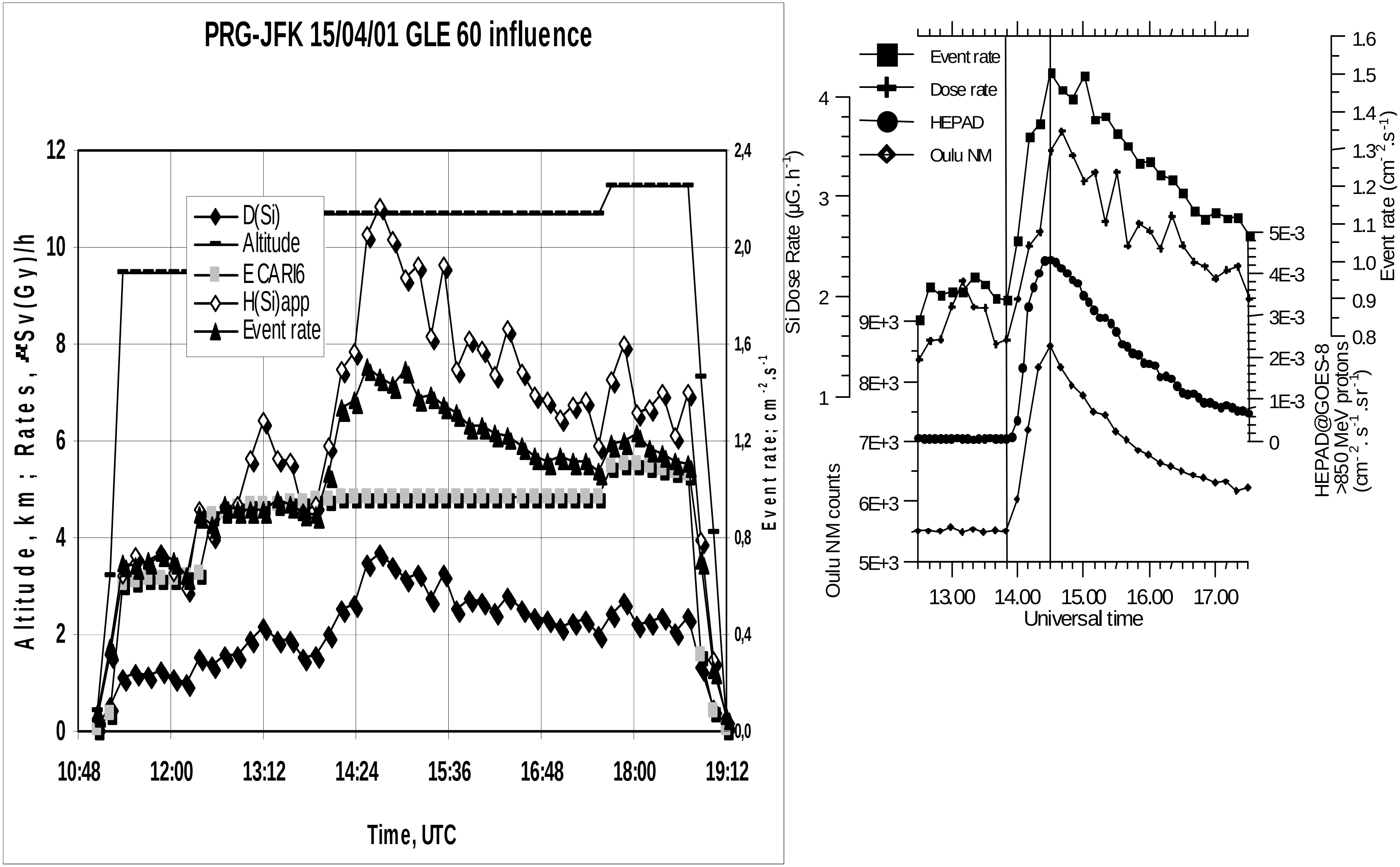

While GLE increase ionisation and dose in the atmosphere, ***strong FD indicate clear depression of the dose measured on airplanes*** *(Spurný et al, SW 2004; Getley et al, SW 2005)*

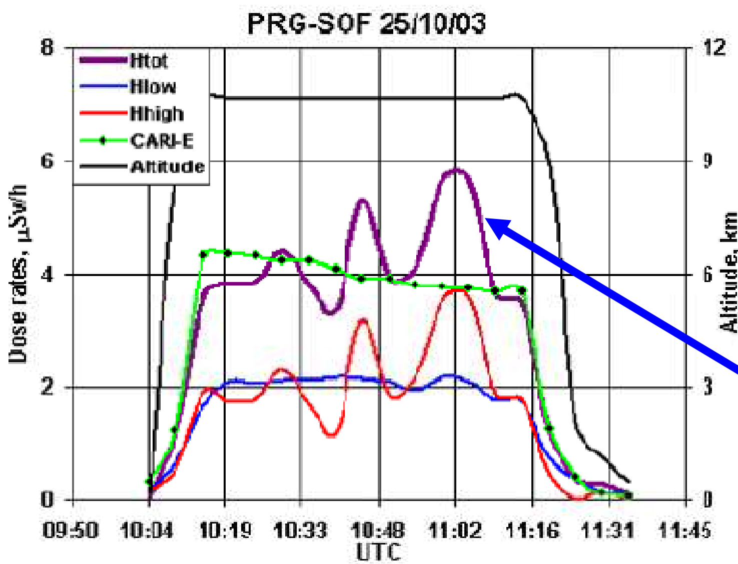

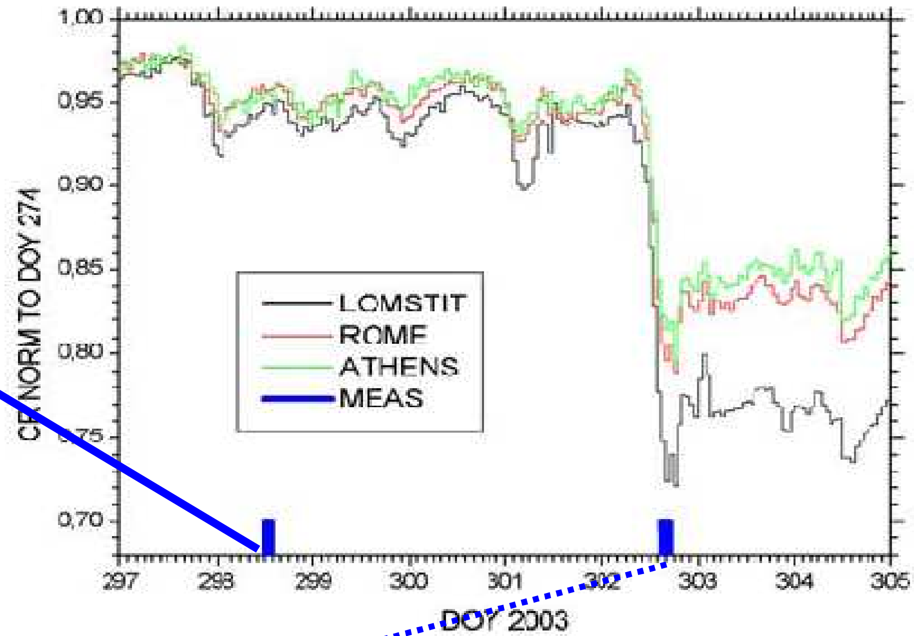

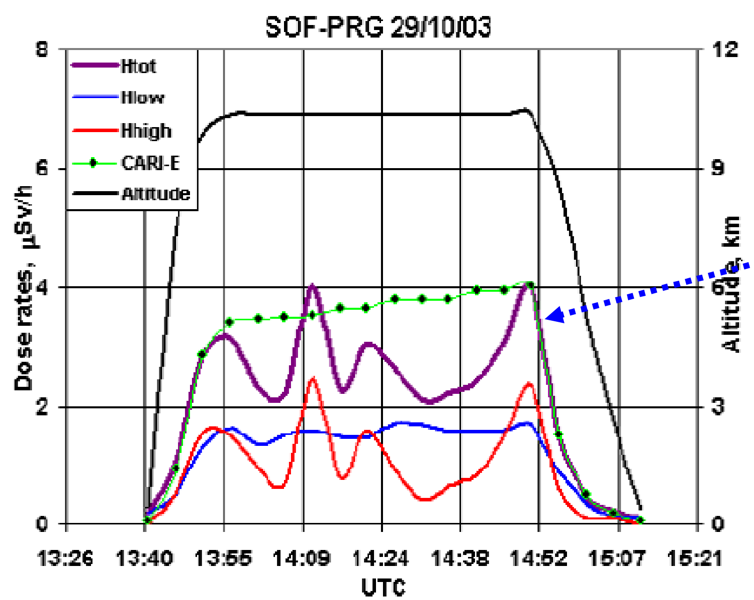

Lantos (RPD, 2005) reviewed doses on airplanes during FDs in 1981-2003 and using NMs he proposed a simplified method to estimate dose variations from GCR variations during FDs.

Dorman et al (AG, 2005b) - ***satellite anomalies*** (220 satellites) found characteristics for quiet and dangerous days (table 1) indicating clear difference in energetic particle fluence.

Satellite anomalies - plasma induced charging (external and internal), sputtering effects, phantom commands, induced mode switching, loss of attitude control/orientation, loss of signal phase and amplitude lock, solar cell degradation and common electronic malfunctions) are listed by *McKenna-Lawlor (2007*).

Table 1. Average characteristics of space weather in days with and without satellite anomalies (1971–1994).

Parameter	"quiet" days (no anomalies)	"probably dangerous" days (anomalies in 1–2 satellites)	"dangerous" days (anomalies in ≥3 satellites)
Total No. of days	5862	2606	298
No. of anomalies (per day, per satellite)	0	1.68±0.04	4.55±0.18
No. of satellites with anomalies (per day)	0	1.24±0.01	3.51±0.06
Daily A_p	14.57±0.18	17.55±0.36	21.15±1.32
Maximal A_p	29.26±0.40	34.46±0.73	40.03±2.53
Minimal D_{st}, nT	−31.78±0.38	−36.49±0.70	−42.68±2.20
Daily proton flux >10 MeV, pfu	0.30±0.09	0.46±0.12	17±12
Maximal proton flux >10 MeV, pfu	8.20±1.70	18.1±4.4	91±30
Electron fluence >2 MeV $(\times)10^7$), cm^{-2}	4.90±0.29	7.59±0.60	12.7±2.7
Solar wind speed, km/s	441.9±1.5	466.2±2.5	500±9
IMF intensity, nT	6.88±0.04	6.98±0.06	6.72±0.18

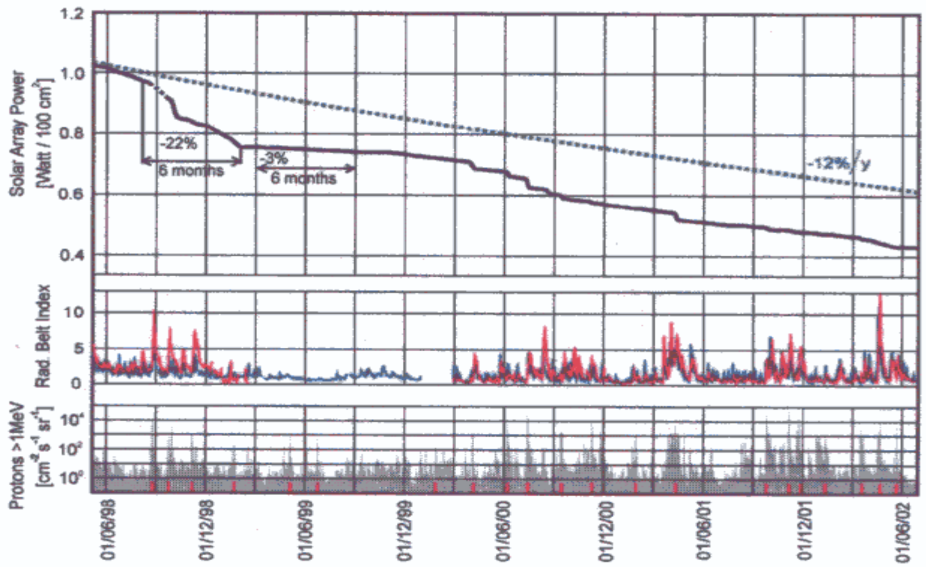

Fig. 2. MAGION-5 solar array degradation during the period from May 1998 to July 2002. The two curves in the central part of the figure show the radiation belt indices based on NOAA POES data: >30 keV (red) and the >300 keV (blue) electrons. Daily proton flux values measured by FOES-8 are shown in the lower panel. Solar proton events are denoted by red marks on the time scale. Note: most of the step-like decreases in the solar cells' output power are connected with strong solar proton events; periods with a steeper decrease in the output power correspond to periods of enhanced radiation belt indices.

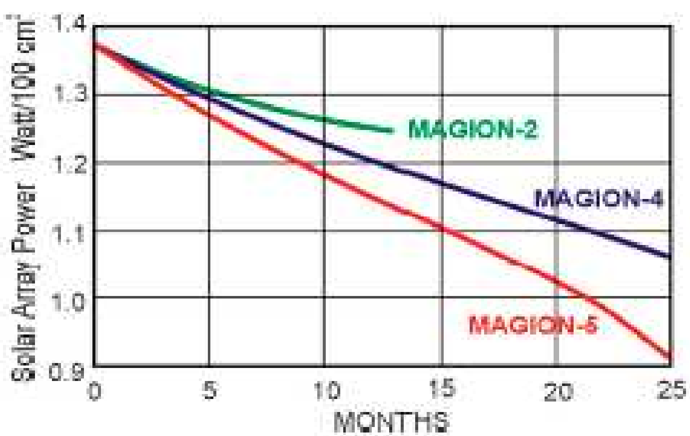

From (*Tříska, P. et al., Ann. Geophys., 23, 3111-3113,2005*):

Magion-5 (subsatellite to Interball-auroral) – ***Energetic p have immediate negative effect on solar array efficiency; step-like decreases in solar array power output***; cases of distinct decreases of power output can be explained by increase of RB particle flux.

Significant difference of solar array power at three subsatellites (almost same construction) at different orbits: highest rate of degradation is for auroral one (Magion-5).

SPE contribute also to the trapped population.

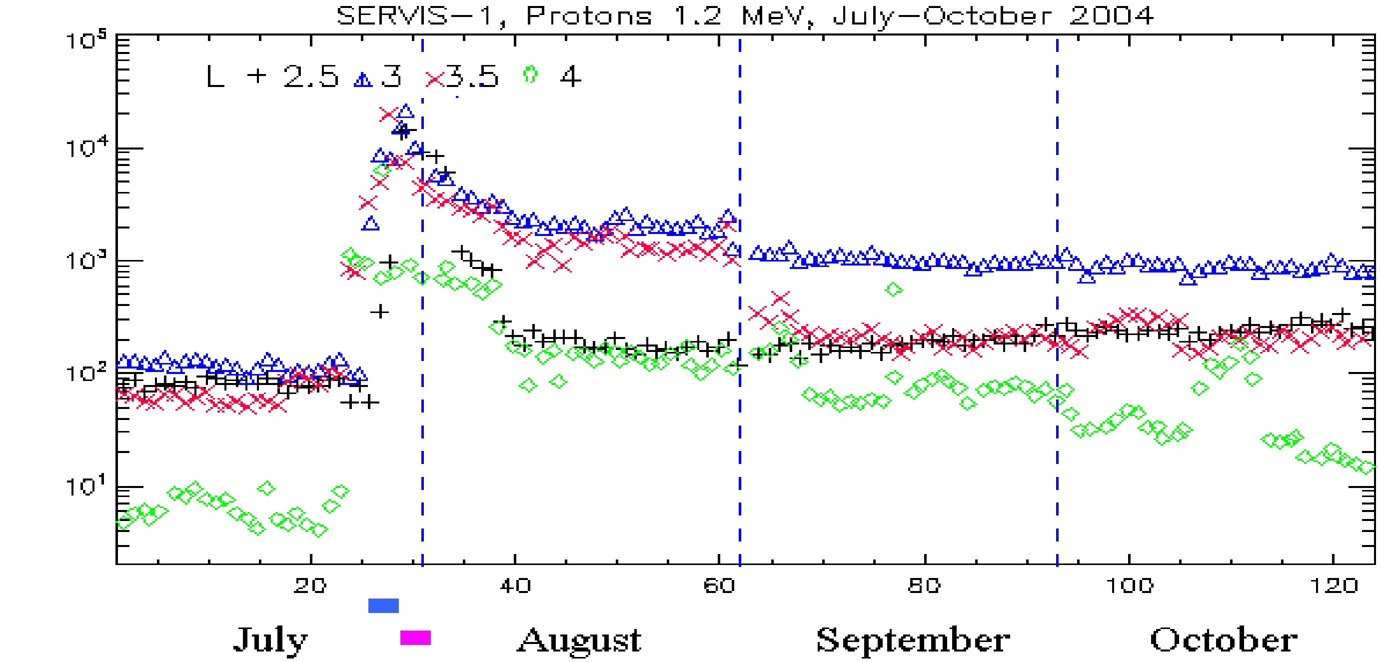

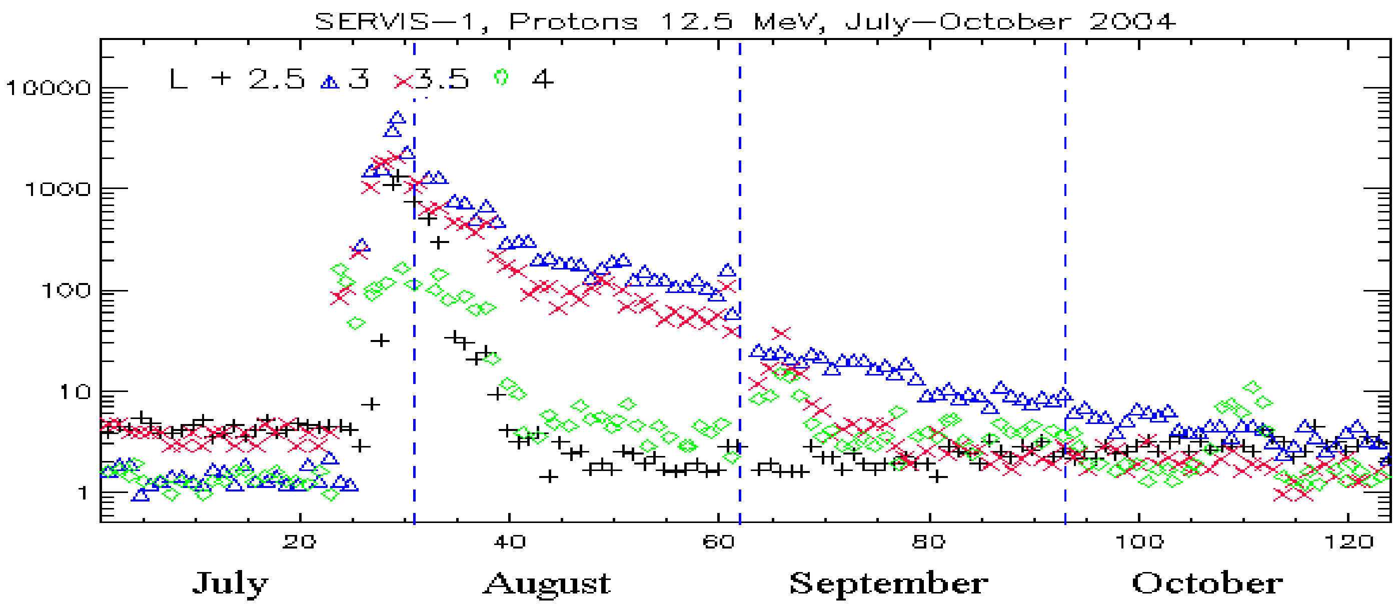

GOES

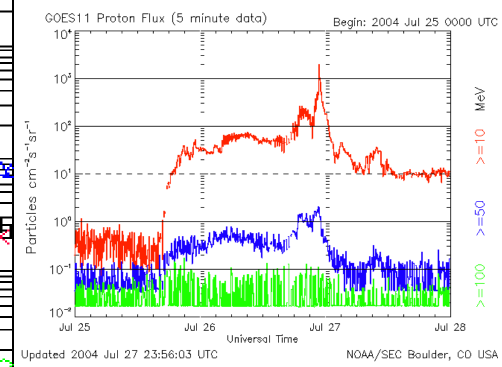

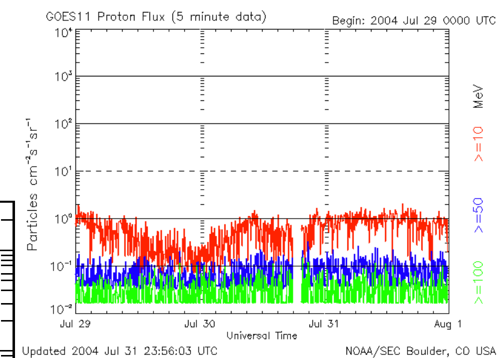

Lazutin, 2011

Significant difference of ***electron energy loss*** with that of proton is *bremsstrahlung (breaking radiation).*

If a *charged particle is accelerated or decelerated*, *it emits electromagnetic radiation* (in the encounter between electron and nuclei of the material). At high energy, for electrons this process is more important than ionisation.

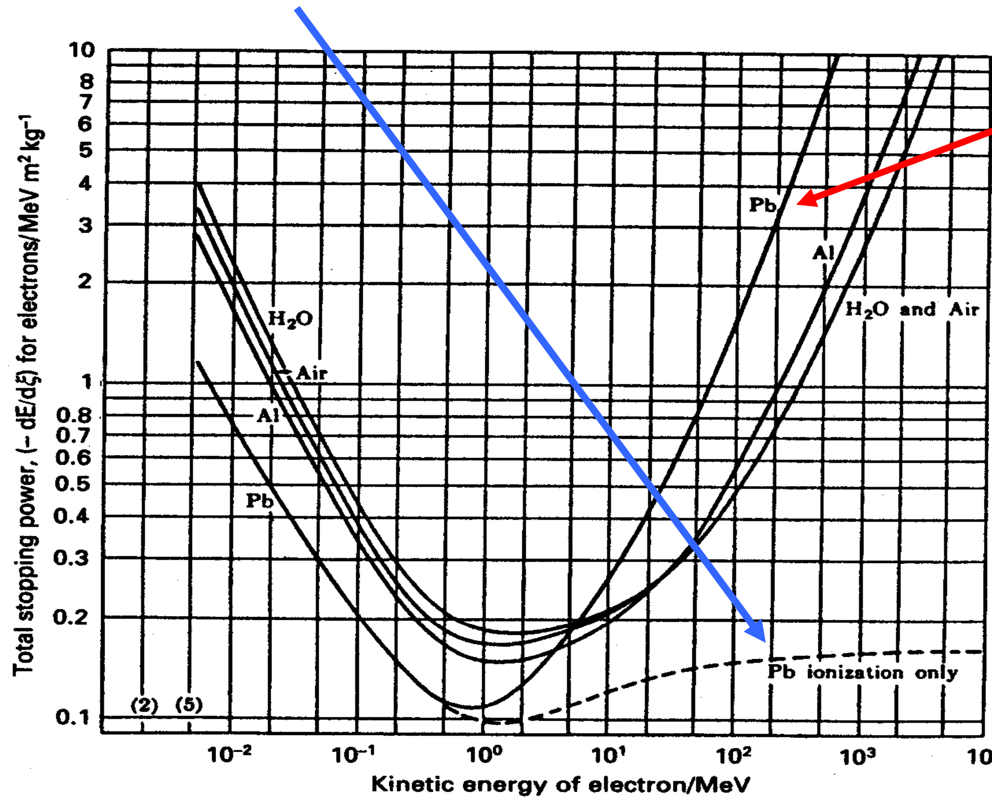

Total rate

of energy loss

Figure 3.5. The total stopping power for electrons in air, water, aluminium and lead. At energies less than 1 MeV, the dominant loss mechanism is ionisation losses. At higher energies, the dominant loss process is bremsstrahlung. For comparison, the contribution from ionisation losses for electrons in lead is also shown. (From H. A. Enge (1966). *Introduction to nuclear physics*, page 190, London: Addison-Wesley Publishing Co.)

Range and stopping power,
different for electrons and protons

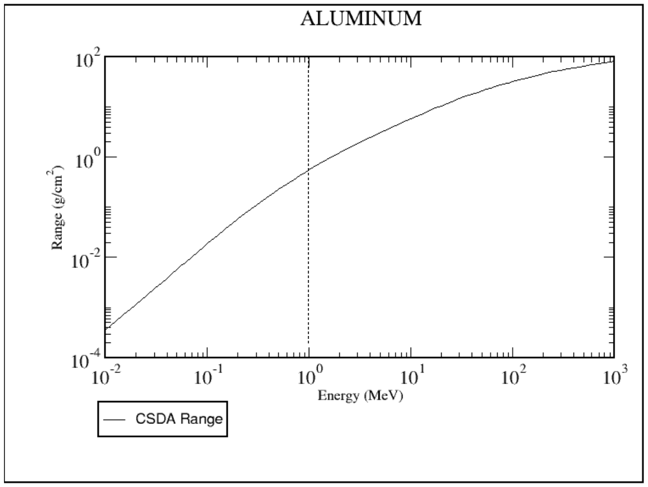

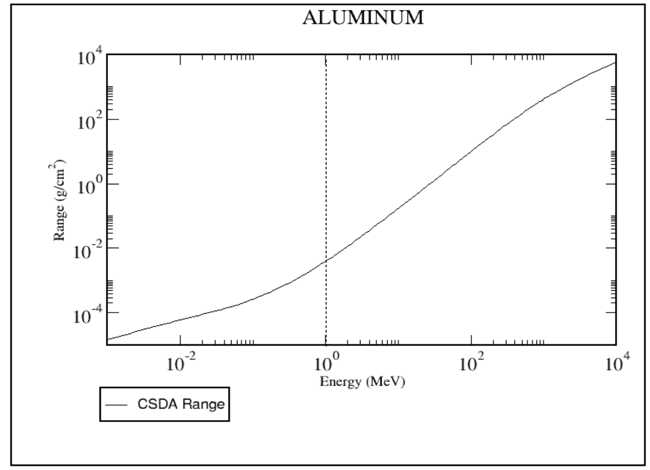

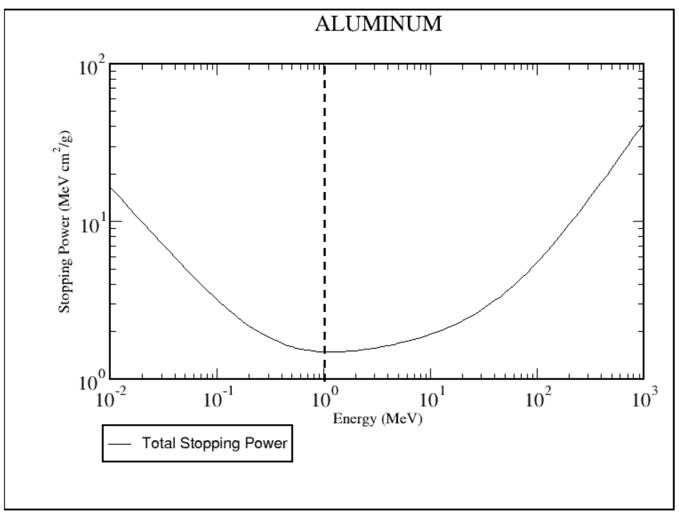

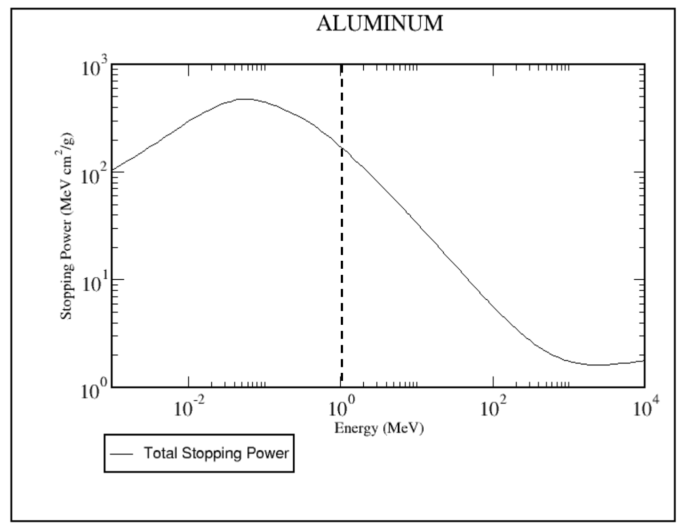

Downloaded from http://physics.nist.gov/PhysRefData/Star/Text/PSTAR.html

Penetration of electrons into the atmosphere.
Production rate of ions is on x axis.

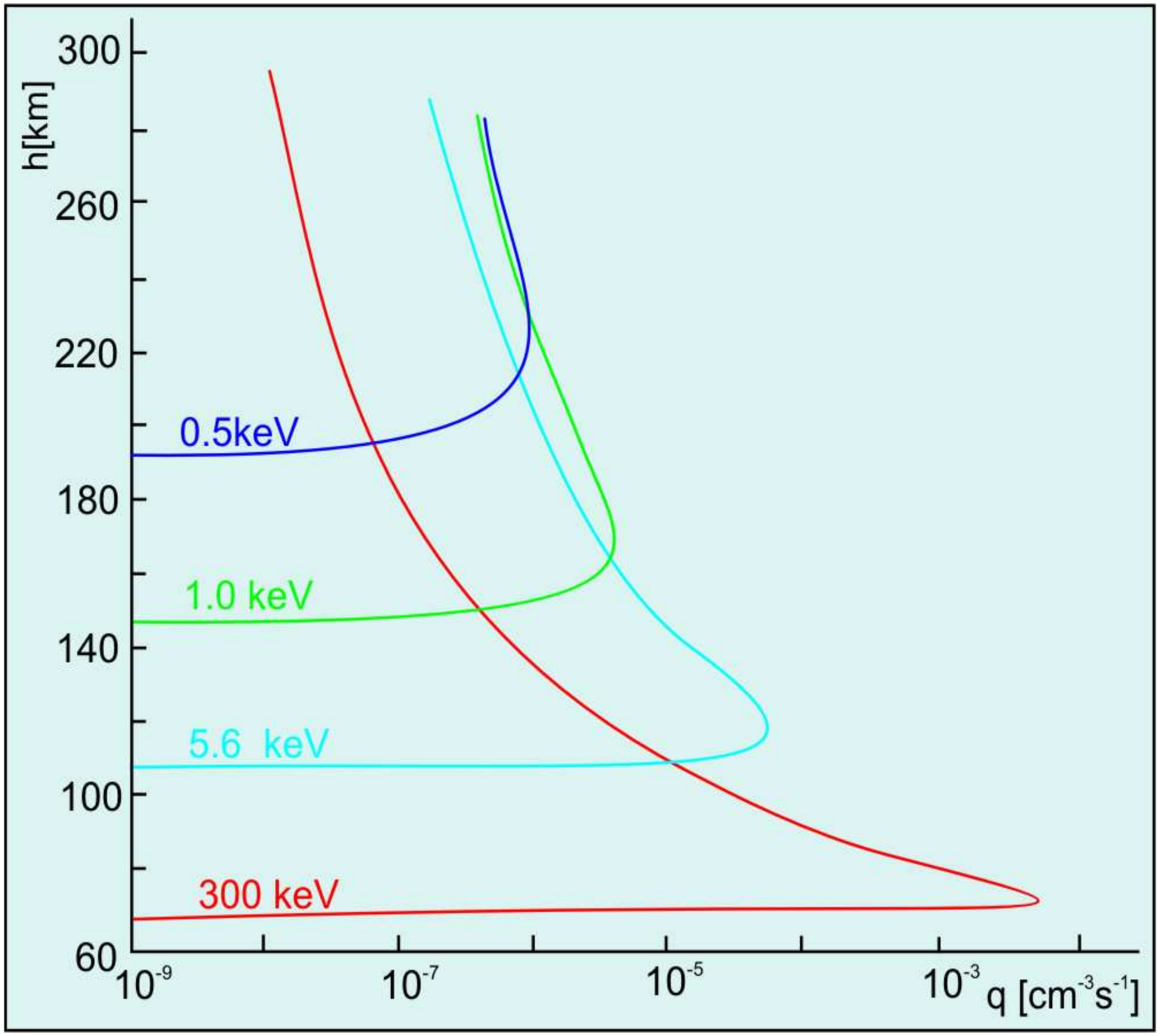

According to *(M.H. Rees, Planet. Space Sci., 11, 1209, 1963)*, the altitude profiles of the rate of ion production in the atmosphere along the 1cm of the electron path has a maximum close to the range of electrons and below that it is abruptly decreasing. The profiles have energy as a parameter. ***For 300 keV the peak is about 70 km, for 40 keV about 95 km, for 6 keV about 110 km.***

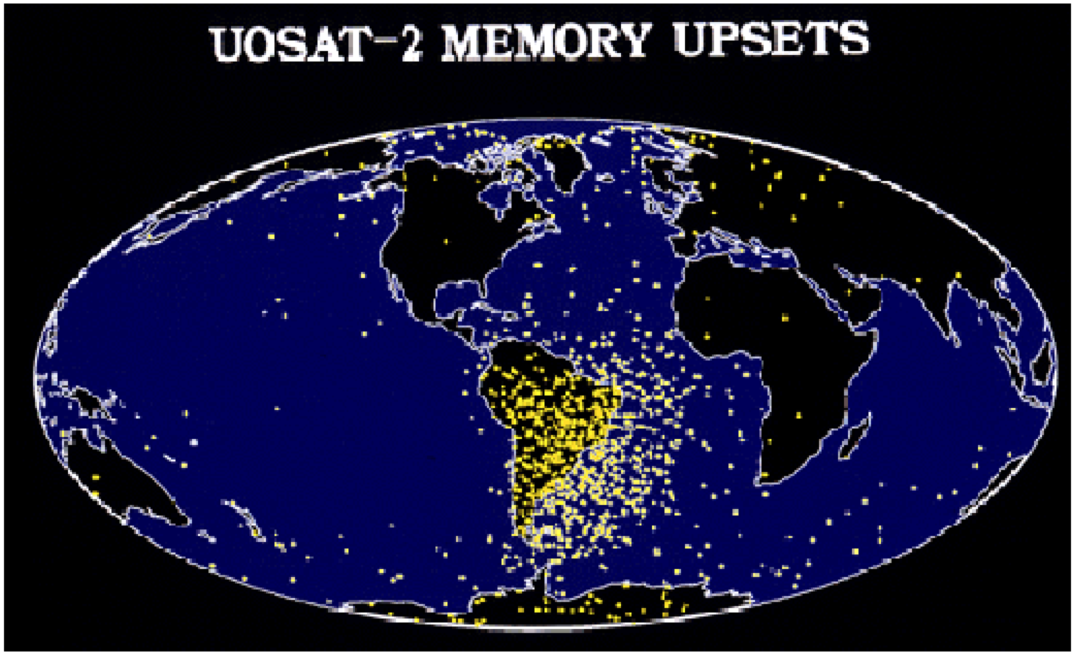

Single Event Upset effects at UOSAT-2 satellite

From F. Nichitiu, 2004,
http://www.lnf.infn.it/seminars/nichitiu.ppt

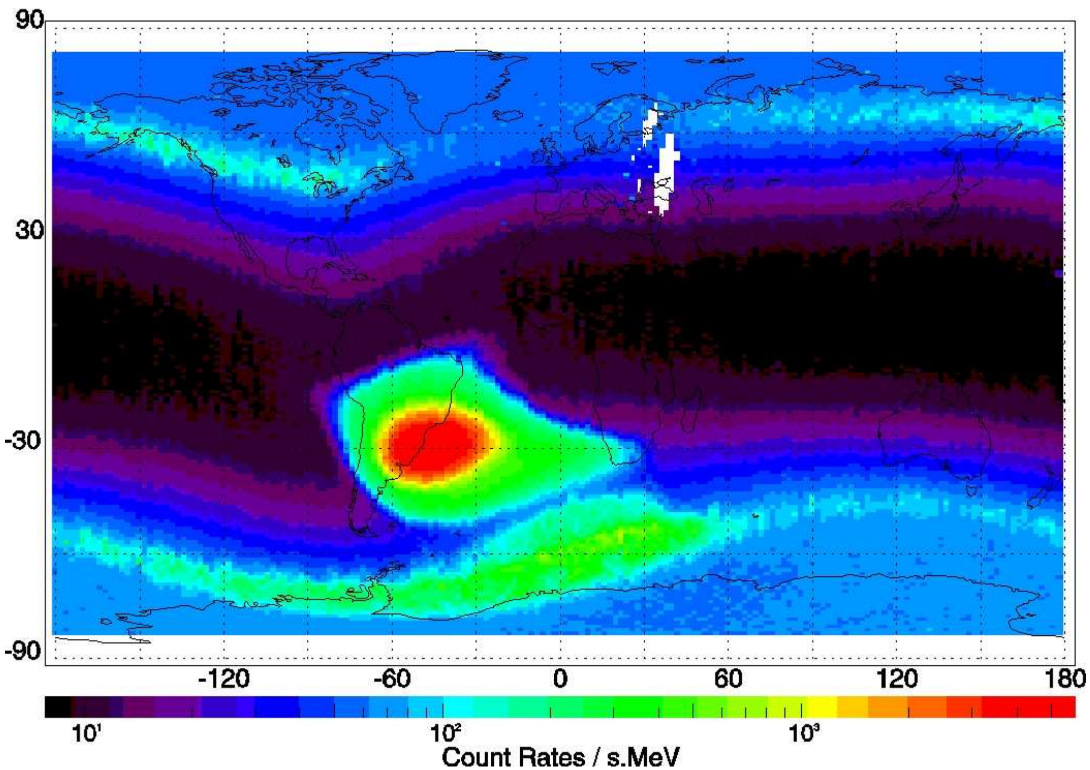

Map of gamma ray flux ~3-8 MeV on 500 km, CORONAS-I satellite,

From (*Bučík, R. PhD thesis, 2004 and Bučík, R. et al., Acta Physica Slovaca, 50, 267-274, 2000*).

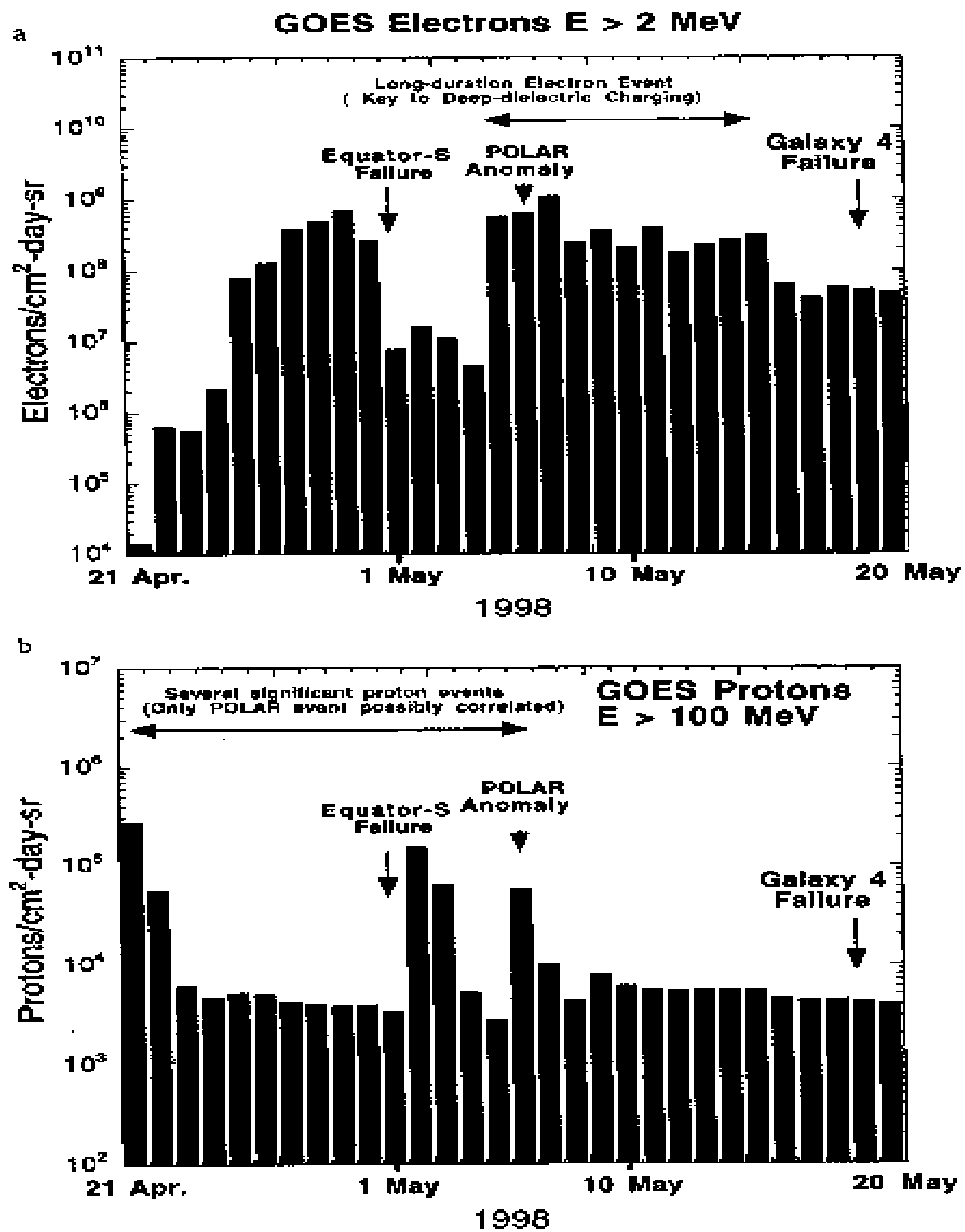

Fig. 3. a) GOES daily flux values of electrons with E>2 MeV for the period from April 21, 1998, to May 20, 1998. Dates of various spacecraft operational problems are noted including the Galaxy 4 failure on May 19. b) Similar to a) but for protons with E>100 MeV (courtesy of H. Singer).

Electrons due to their penetration ability into materials (cables, inner spacecraft system) are dangerous for satellites. Deep dielectric charging.

From (*Baker, D.N. et al., Disturbed space environment may have been related to pager satellite failure, Eos, 79, 477, 1998*)

Surface charging anomalies occur at places where energetic electrons are injected to geostationary orbit (from Rice University and NOAA web sites).

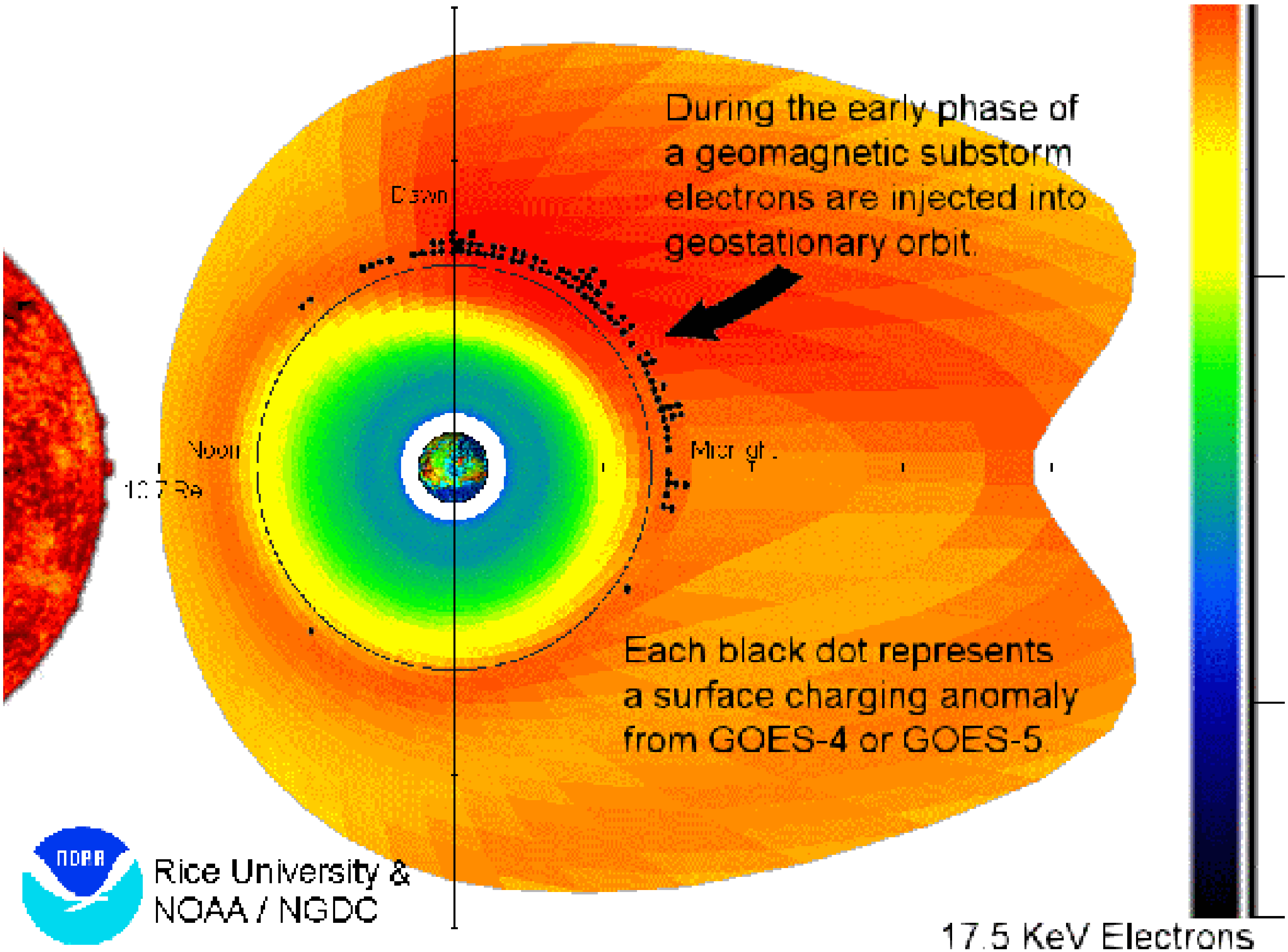

3. Indirect relations of Cosmic Rays to Space Weather studies.

3.1. Short term alarms before radiation storms.

Ions - ***tens to hundreds MeV*** cause the ***main radiation damage*** on satellites during solar radiation storms – failures of electronic elements, communication and biological consequences.

Before their massive arrival, NM, if with good temporal resolution and network in real time is working, may afford ***useful warning few minutes – tens minutes before (Dorman, 2005).***

a. NM at a single site (***high latitude, good statistics***) allows to obtain energy spectra of solar CR: South Pole, combining NM64 and monitor without Pb (*Bieber, AOGS, 2006*) event 20. january 2005.

Su Yeon Oh et al, ICRC, 2009 checked the potential of South Pole NM data for prediction of radiation storm intensity measured by GOES. The energy spectrum was estimated.

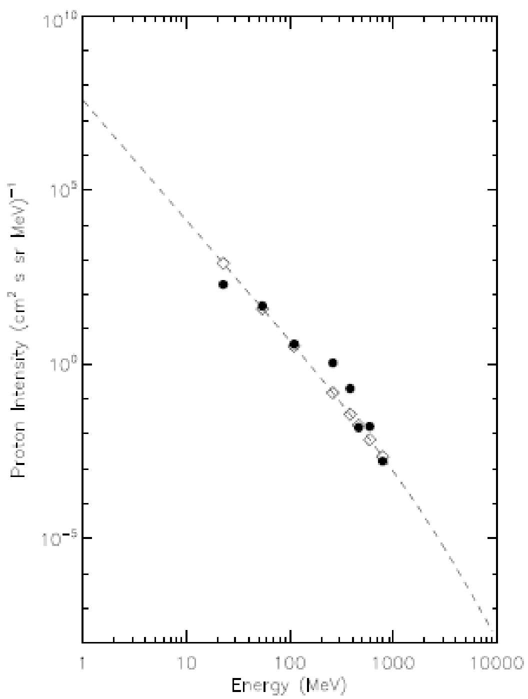

Fig. 1: Energy spectrum of the SPE of July 14, 2000 (Bastille event). The dashed line is the spectrum derived from neutron monitor observations at the *time of the neutron monitor peak.* Filled circles are 8 GOES channels plotted at the mean energy of the channel at the *time of the peak for the corresponding GOES channel.* Open diamonds are the predicted proton intensity of the GOES channels, derived by extrapolating the neutron monitor spectrum downward in energy.

TABLE I: Linear and Logarithmic Correlation Coefficients. Left: Correlation coefficients between observed and predicted peak intensity of proton channels. Right: Correlation coefficients between observed fluence of proton energy channel and predicted intensity of proton energy channel.

Proton	Energy Range	Peak Intensity		Fluence	
Channel	(MeV)	Linear	Logarithmic	Linear	Logarithmic
P4	15-40	0.0132	0.4091	-0.0504	0.4093
P5	40-80	0.2336	0.5113	-0.1058	0.3763
P6	80-165	0.8631	0.7543	-0.0203	0.5037
P7	165-500	0.9376	0.8687	0.0386	0.5888
P8	350-420	0.9919	0.9758	0.6903	0.8196
P9	420-510	0.9991	0.9661	0.7090	0.8335
P10	510-700	0.9996	0.9823	0.8346	0.8665
P11	$>$ 700	0.9992	0.9834	0.9657	0.9088

SP GLE observations can be used to predict radiation intensity of the higher energy proton channels from GOES.

b. NM network at high latitudes.

GLE alarm in real time – Spaceship Earth – 9 out of 10 GLE in 2001-2005 provide alarms. ***with earlier warning than satellite system*** (SEC/NOAA).

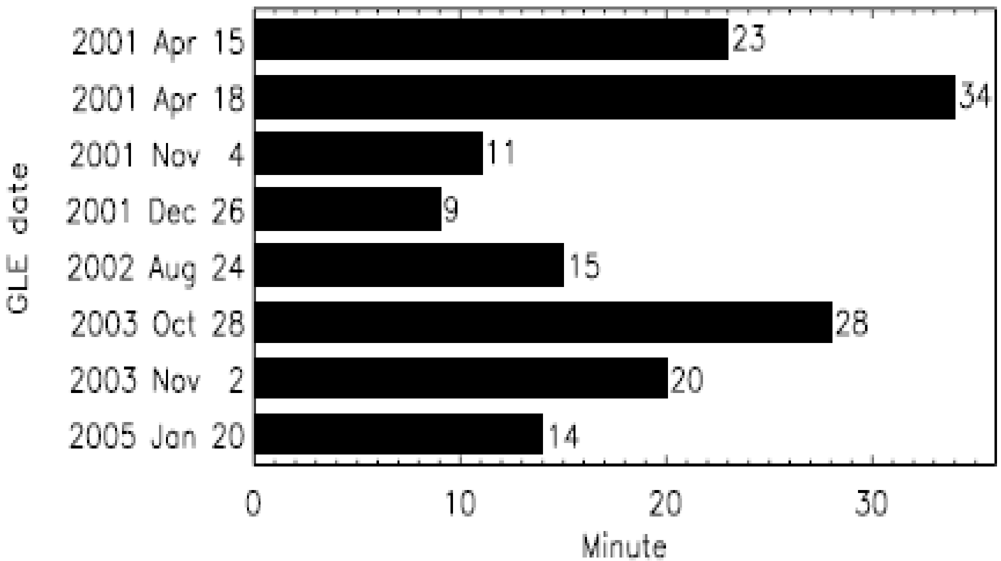

Figure 5. Number of minutes by which GLE alert precedes earliest SEC proton alert.

Kuwabara et al, 2006

c. Including NM at various cut-offs.

Several steps of GLE alert algorithm using NM network described by *Mavromichalaki et al., 2009.* NMDB project of 7FP EU.

Table 3
Comparison of the GLE alarm times from our system to the alarm times on the basis of satellite proton data.

GLE number	Event date	Flare time (UT)	Location	Flare's type	GOES alert (100 MeV, >1 pfu)	Stations GLE alert (UT)	Difference of the two
60	15 April, 2001	13:19	S20W85	2B/X14.4	14:21	14:07	14
61	18 April, 2001	02:11	S20WLimbb	C2	3:11	2:51	20
64	24 August, 2002	00:49	S02W81	1F/X3.1	1:48	1:44	4
65	28 October, 2003	09:51	S16E08	4B/X17.2	11:51	11:18	33
66	29 October, 2003	20:37	S15W02	2B/X10.0	–	NO GLE	–
67	2 November, 2003	17:03	S14W56	2B/X8.3	17:56	17:46	10
68	17 January, 2005	–	–	–	–	NO GLE	–
69	20 January, 2005	06:36	N14W61	2B/X7.1	7:04	6:56	8

TABLE III: NMDB stations contributing to GLE Alert on-line

Almaaty	Jungfraujoch, NM64	Norilsk
Apatity	Kerguelen	Novosibirsk
Athens	Kiel	Oulu
Aragats	Lomnicky stit	Rome
Nor-Amberd	Mobile Cr lab	Terre Adelie
Irkutsk	Magadan	Tixie Bay
Mt Hermon	Moscow	Yakutsk
Jungfraujoch, IGY	Mirny	

From Souvatzoglou et al., 2009

Anashin et al, ICRC, 2009 – development of alert signal for GLEs.
http://cr0.izmiran.ru/GLE-AlertAndProfilesPrognosing

d. Energetic electrons from flares.

Posner, 2007 – ***possibility of short term alarm from relativistic solar electrons.***

New results:

http://ccmc.gsfc.nasa.gov/RoR_WWW/workshops/2010/Tuesday_pdf/Posner_REleASE_CCMCWS_final.pdf

(Jan. 20, 2005) – e precursor observed 20-25 min before radiation storm.

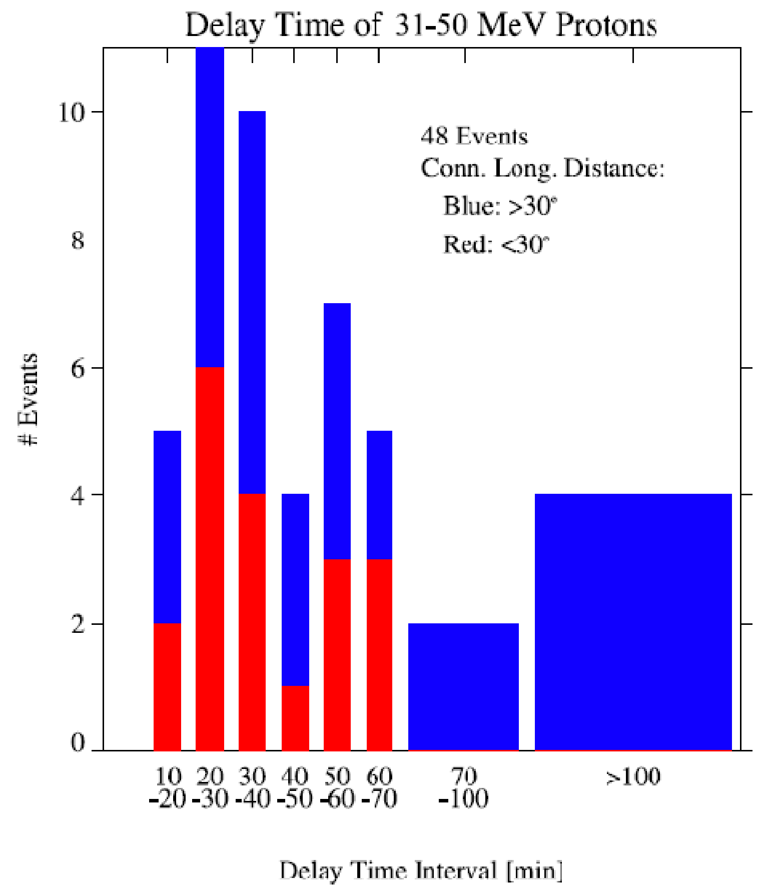

Figure 3. Histogram shows the distribution of 31–50 MeV proton onset delays over relativistic electrons. The diagram uses 48 SEP events from 1996–2002 with their observed delay times.

e. High energy n, gamma from the Sun.

On the ground:

Solar Neutron Alert: http://cr0.izmiran.ru/SolarNeutronMonitoring

Low altitude satellite(s). Example: CORONAS-F (500 km, polar), SONG.

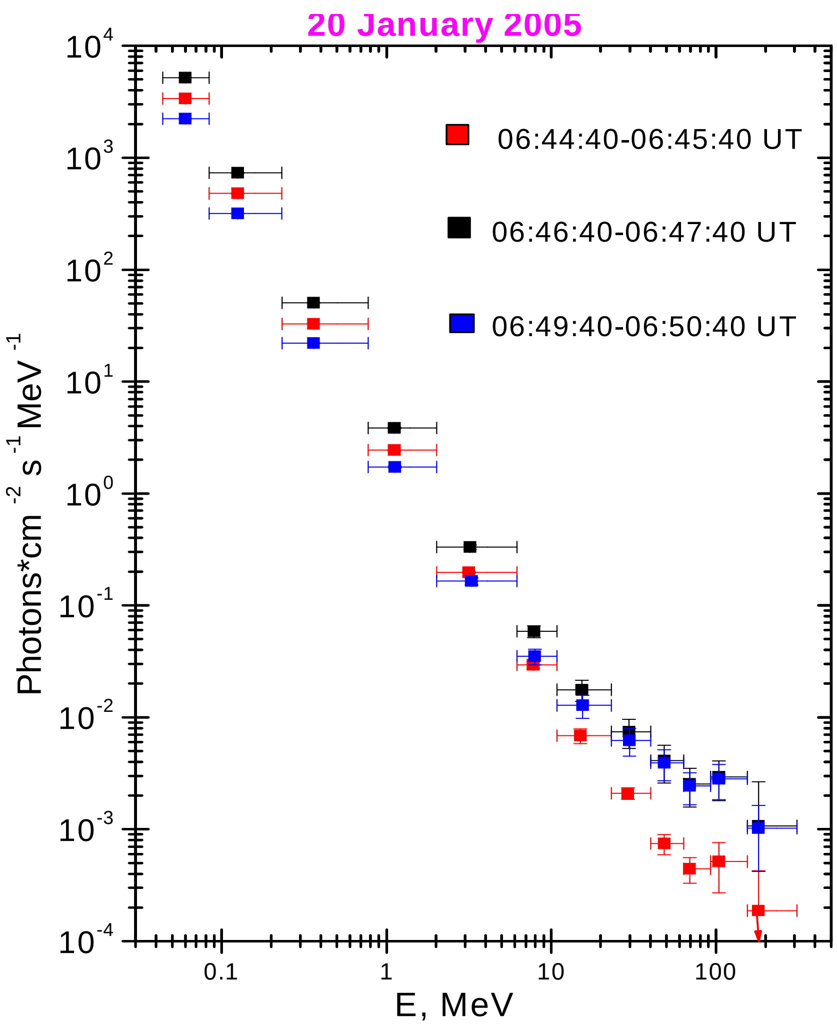

The observation of a broad 70-100 MeV excess, associated with π^{0} decay ***indicates exact time of energetic p appearance in the solar atmosphere***.

Kuznetsov,S.N. et al., 2007, 2011.

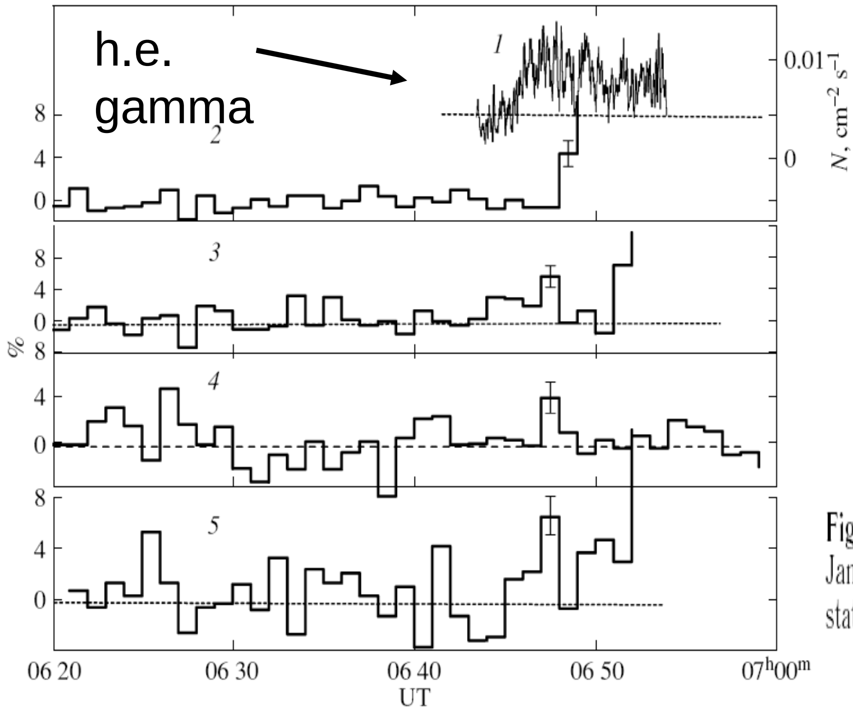

Tool for identification of onset time of *p* acceleration to HE *(Kurt, Yushkov and Belov, 2010).*

Main SCR increase is preceeded by statist. signif. precursor at individual NM.

SONG on CORONAS-F.

Fig. 1. Count rates of gamma-ray emission with an energy >60 MeV (curve *1*, the right scale) and some NMs during the January 20, 2005 event. Curves *2*, *3*, *4*, and *5* correspond to the South Pole, Oulu, Baksan, and Norilsk, respectively. The statistical errors of the NM count rates are given in these and subsequent figures.

Table 3. Basic characteristics of the events

Parameter	GLE 48	GLE51	GLE52	GLE65	GLE69
Date	May 24, 1990	June 11, 1991	June 15, 1991	Oct. 28, 2003	Jan. 20, 2005
Coordinates	W76 N36	W17 N31	W69 N33	E08 S16	W61 N14
Onset time of “pion” gamma-ray burst	20:48:30	02:12:56	08:15*	11:03:51	06:45:30
Precursor recording time	20:49–20:50	2:16–2:18	8:20–8:21	11:09–11:10	06:47–6:48
Δt, s	60 ± 30	240 ± 60	330 ± 30	250 ± 30	120 ± 30
Magnitude of effect	6.6σ (Mt. Wellington)	3.5σ (Newark)	8.5σ (Kiev)	2.7σ (Cape Shmidt, Irkutsk)	5σ (Norilsk)
GLE onset time	21:02–21:03	02:35–2:40	>8:30	11:12–11:13	06:49–6:50

* The time corresponds to the first radio emission maximum.

f. Short – term warning of SEP based on position, size of flare.

Laurenza et al., Sp. W., 2009 developed a technique to provide short-term warnings of SEP events that meet or exceed the Space Weather Prediction Center threshold of J (>10 MeV) = 10 # $cm^{(-2)}$ $s^{(-1)}$ $sr^{(-1)}$. The ***method is based on flare location, size, and evidence of particle acceleration/escape as parameterized by flare longitude, time-integrated soft X-ray intensity, and of type III radio emission 1 MHz***, respectively. In this technique, ***warnings are issued 10 min after the maximum of >= M2 soft X-ray flares***.

3.2. Relativistic electron variability.

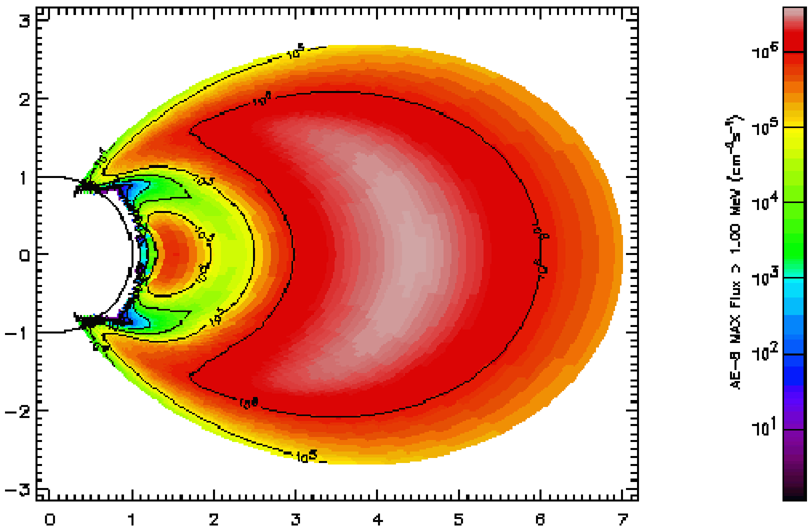

Strong time variations

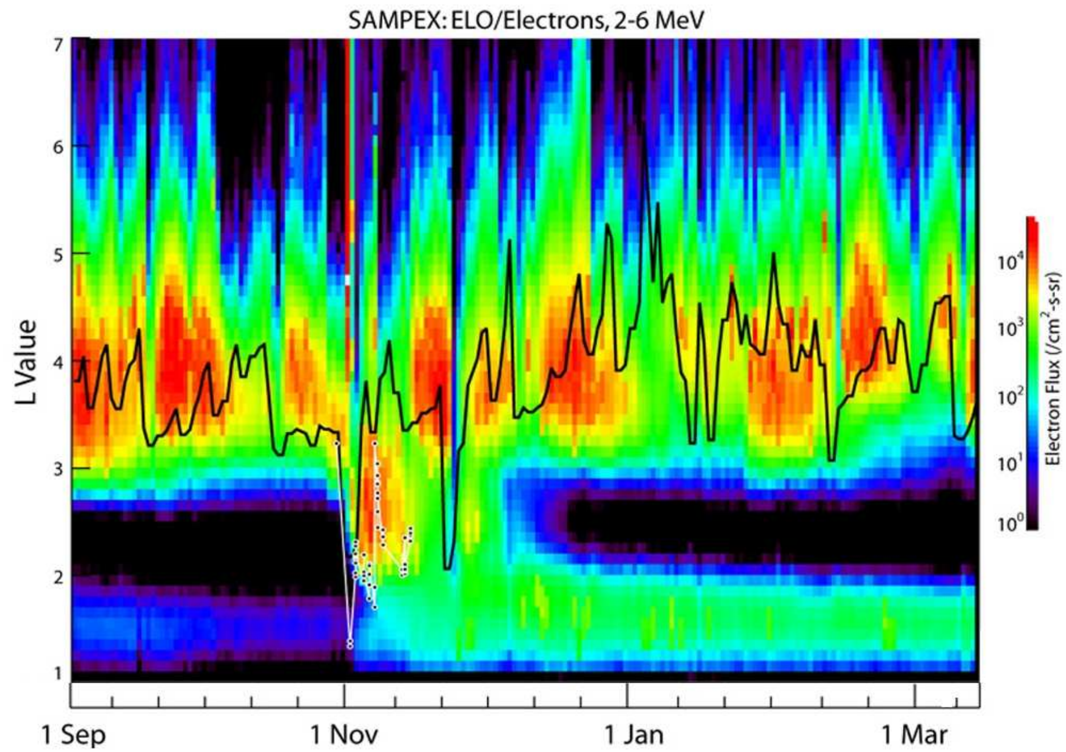

Models (static)

Strong changes of ***e*** populations in outer belt during storms (*CORONAS-F, also CRRES)*

Measurements SAMPEX

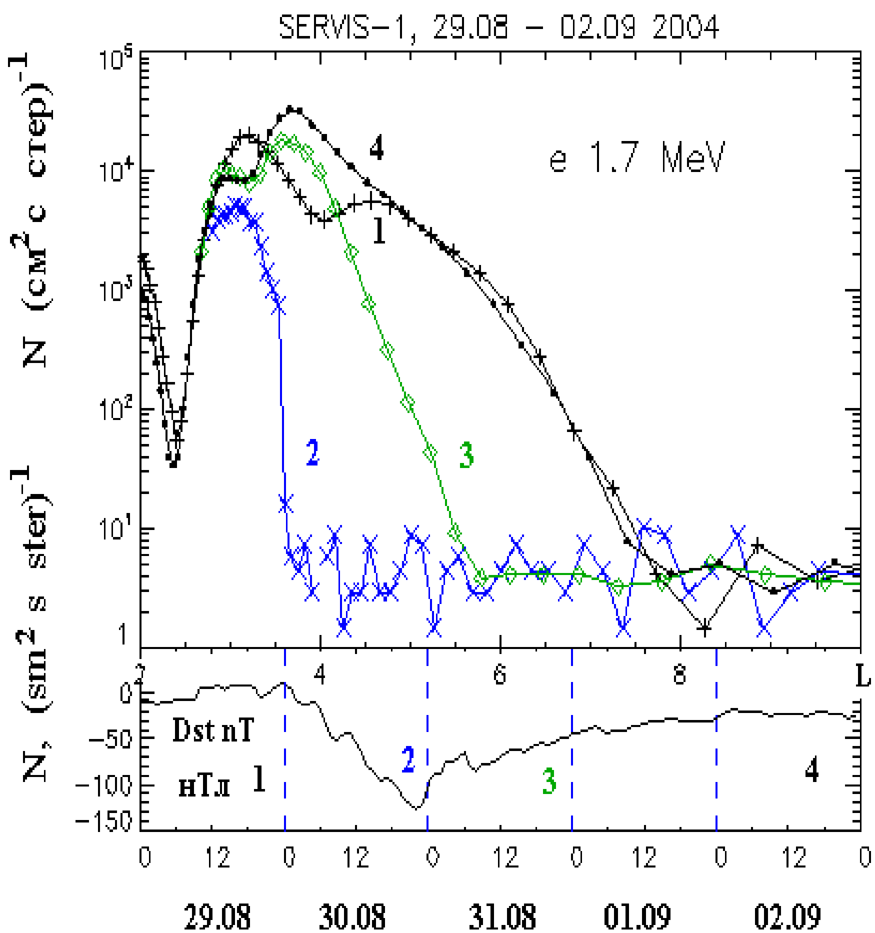

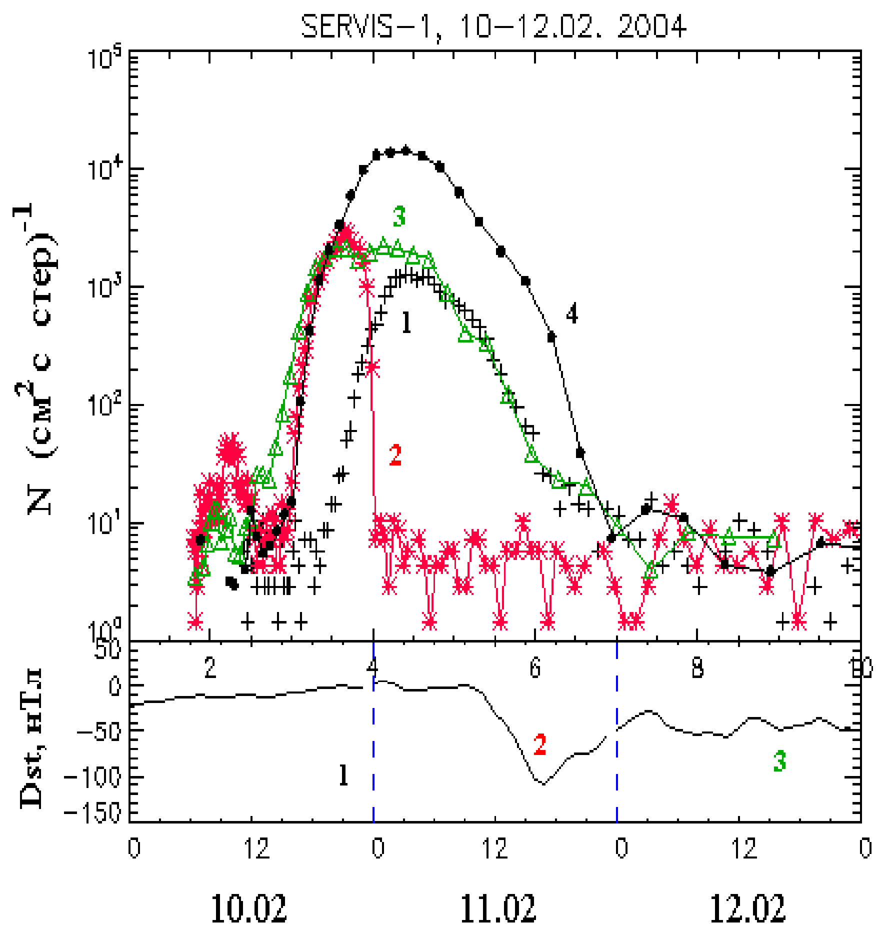

Strong variability: place, time, mutual importance of mechanisms of acceleration and losses the e population is varying inside magnetosphere. SERVIS-1 (JP), 1000 km.

Lazutin et al., 2011.

[Reeves et al., 2011] by extensive analysis confirmed that the geosynchronous relativistic ***e*** flux (1.8-3.5 MeV) is best correlated with the solar wind velocity measured 2 days earlier. ***<u>However, the dependence is not linear, high fluxes are observed for various sw velocities (triangle distribution).</u>***

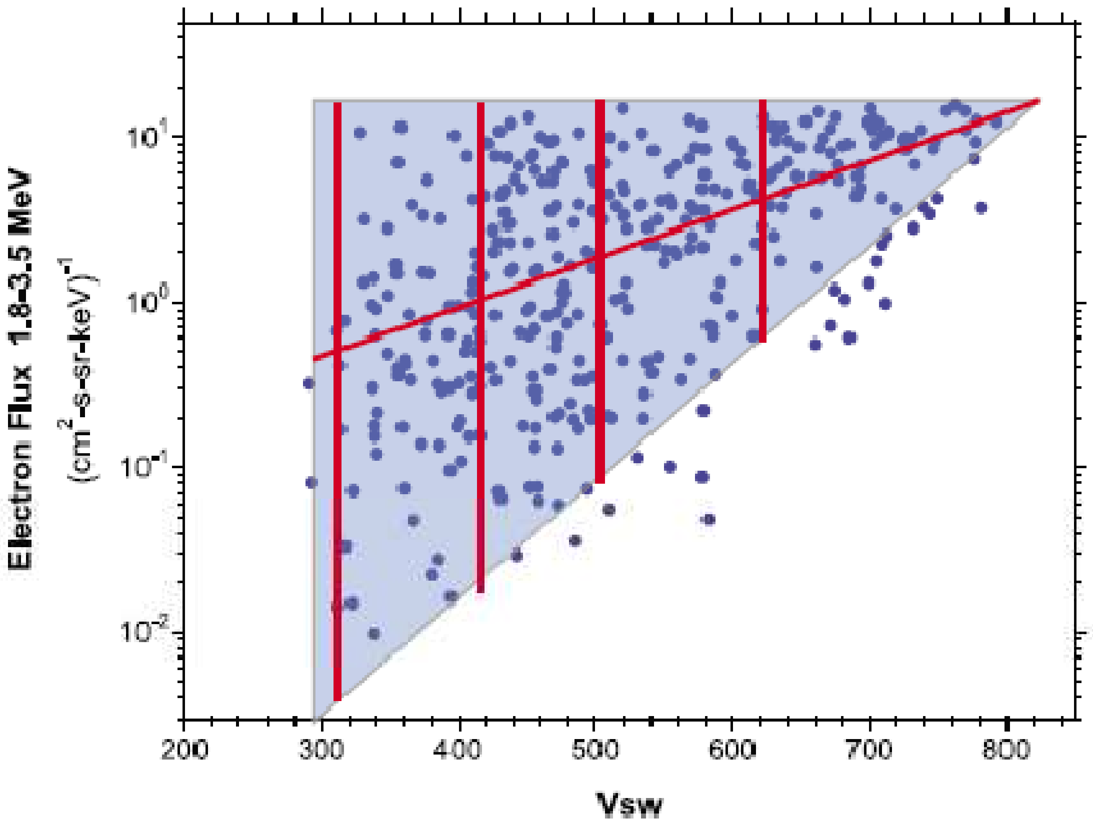

Recently, the cross-correlation of energetic ***e*** flux at low orbit (low equatorial pitch angles) vs sw speed, Kp etc using SERVIS-1 data (>0.3 MeV).

Preliminary example (L=4, 448 points in years 2002-2004, 0.3-1.7 MeV):

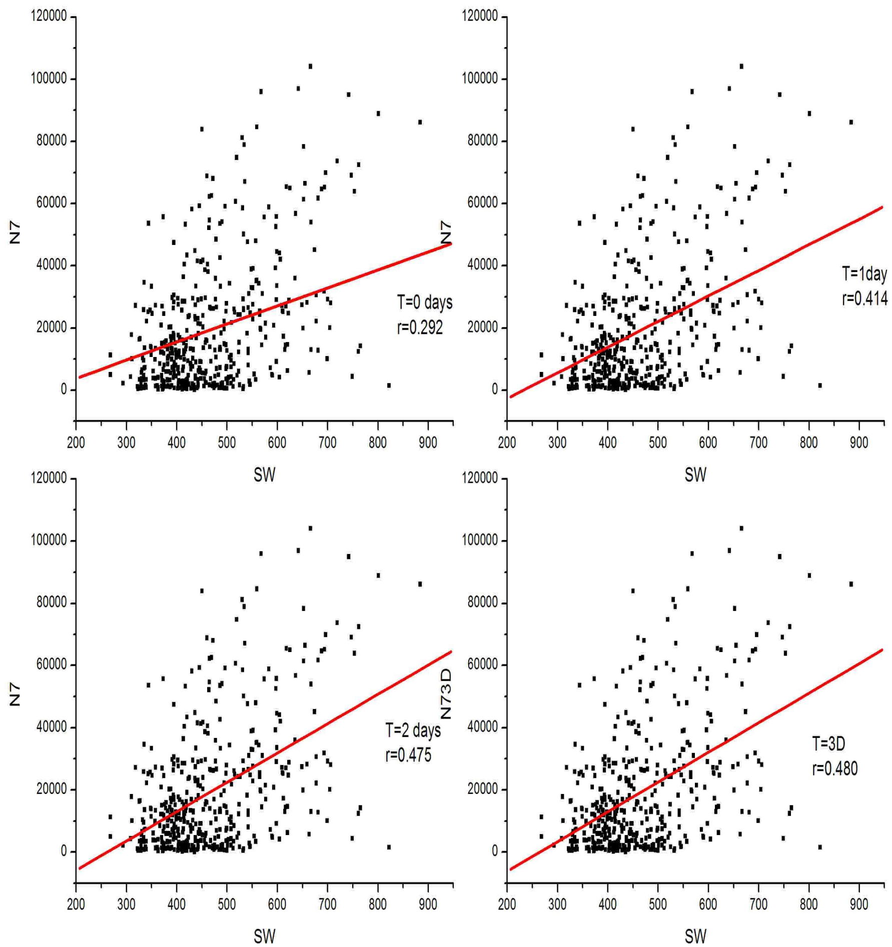

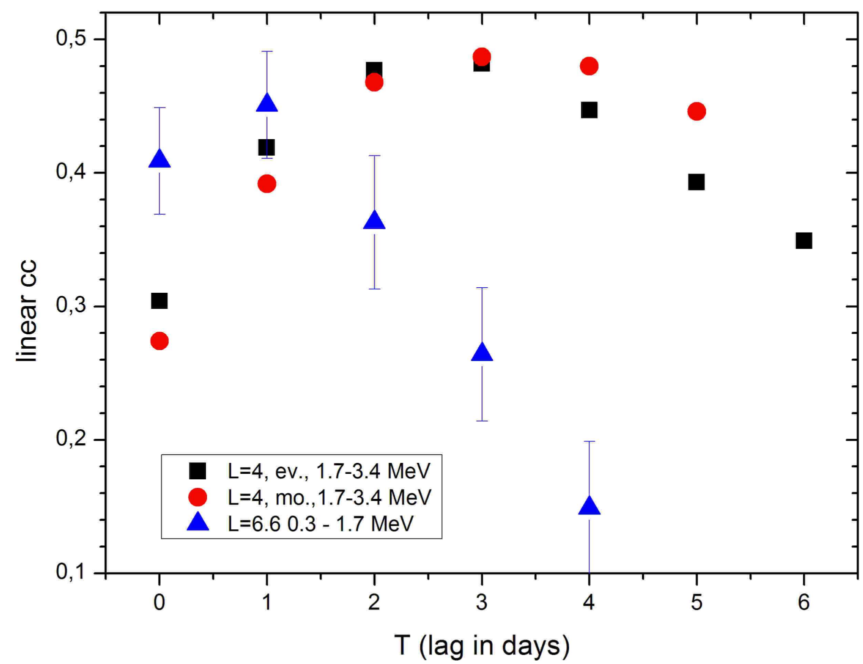

Event in February 2011

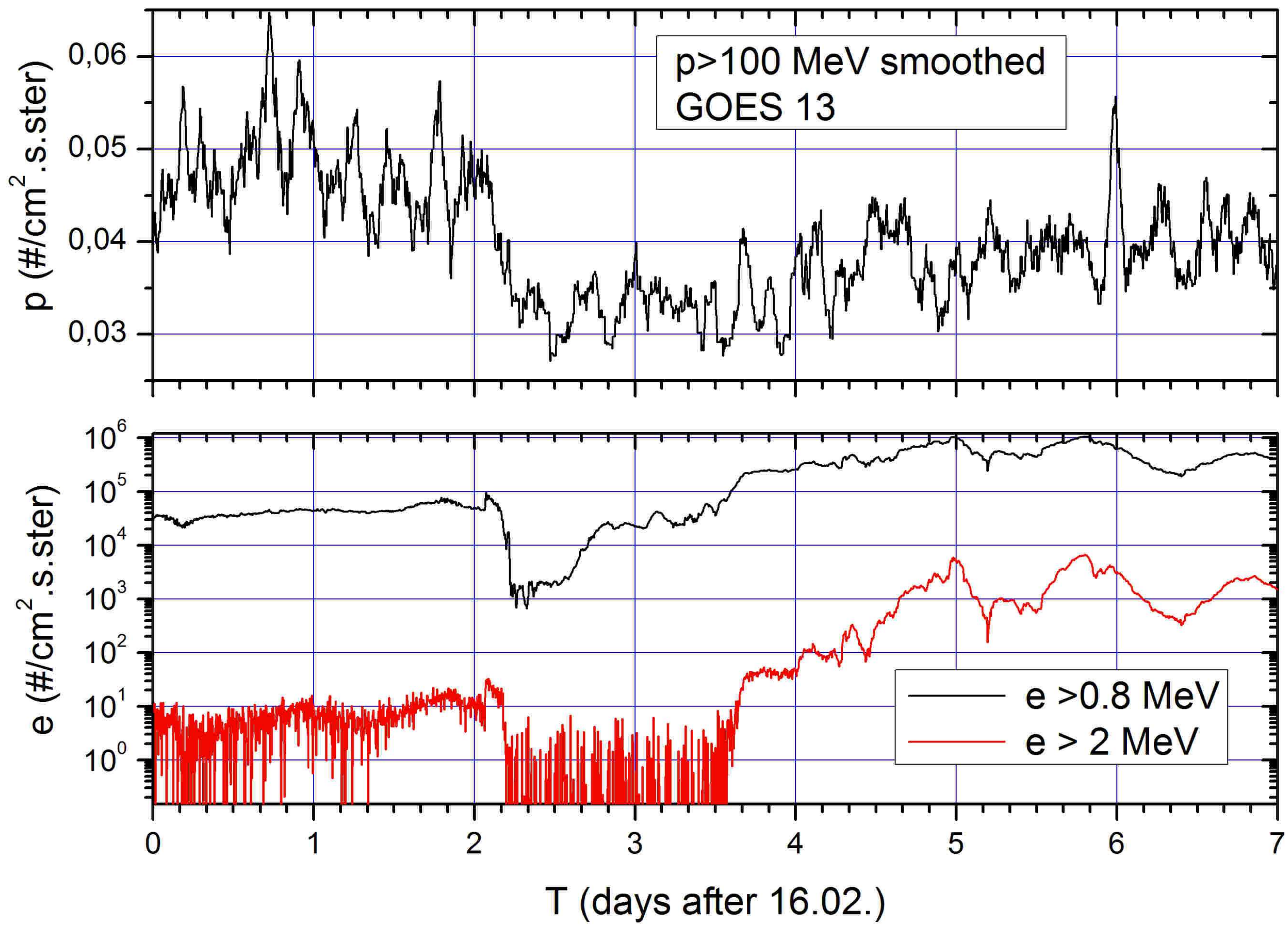

Increase of ***relativ. Electrons up to >2 orders*** after storm

3.3. CR as precursors of geoeffective events.

NMs show ***precursors before arrival of IP shock to Earth and before FD*** (*Dorman, 1963*). Time evolution of Dst and FD are sometimes strongly different *(e.g. Kudela and Brenkus, 2004; Kane, 2010).*

Reviews on relations CR to Space Weather (*Flückiger ECRS, 2004*; *Storini ECRS 2006, 2010*; *Kudela et al, 2000; 2009; Siingh et al., 2010*).

Because CR has high **v** a λ_{par}, ***information about created anisotropy related to IMF inhomogenities is transmitted fast to remote sites (Earth)*** : CR deficit is observed down to $0.1 \cdot \lambda_{par} \cdot \cos(\Phi)$, Φ – IMF angle (*Ruffolo, Ap.J., 1999*).

Precursors of FD near shock depend on magnetic turbulence, mean free path and decay length for energies to which NM and muon detectors (MD) are sensitive.

Typically ***NM ~4 hr before shock arrival ,***

MD ~15 hr before shock (*Leerungnavarat et al, Ap.J., 2003*).

a. <u>Example.</u>

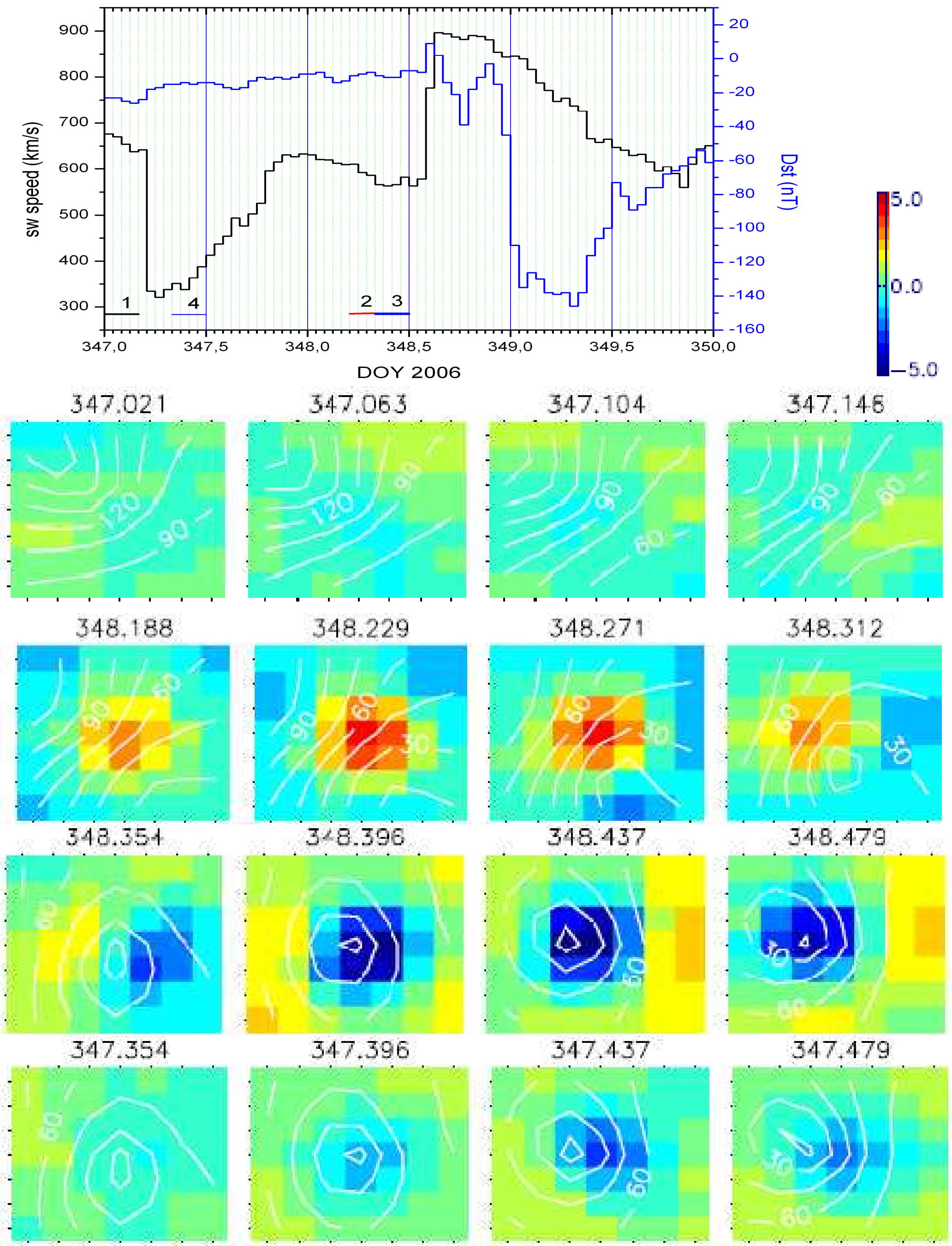

Precursor to FD 14.12.06.
GMDN (*Fushishita et al., 2009; Ap.J., 2010*)

1- before storm ~ isotropy

2 – excess at PA 30-90º – CR is reflected from IP shock approaching the Earth

3 - LC precursor, deficit at PA ~ 0º

4 – weak LC indication *<u>a day before</u>* (~7 h after CME release from Sun, shock at ~0.4 AU).

b. Statistical studies.

2001-2007, before geomagnetic storms. Data GMDN.
(Rockenbach, M. et al., GRL, 2011 in press)

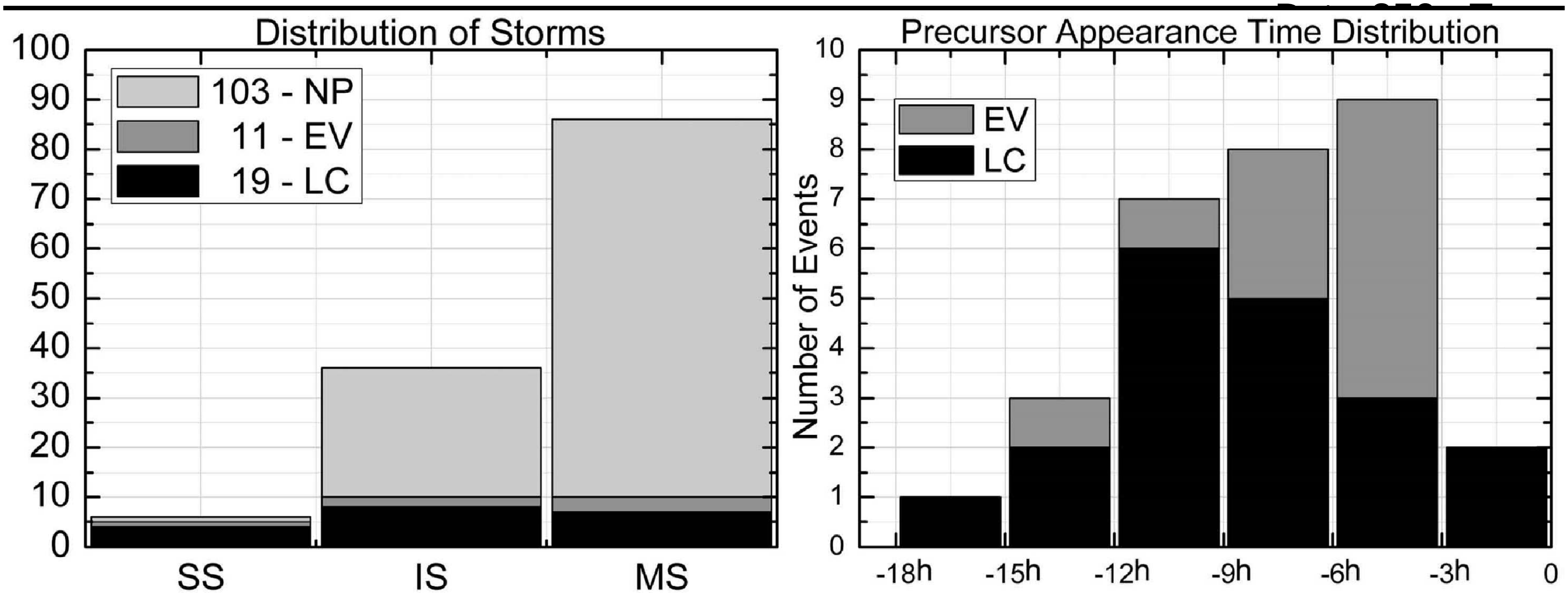

Occurrence of precursors ***before SSC*** increases with $|Dst_{max}|$:
15% for MSt, 30% for IS and 86% for SuperStorms is accompanied by CR precursor observed in average ~ ***7.2 h before the storm onset*.**

Few open questions:

-May CR provide informations about validity of geomagnetic field models during strongly disturbed conditions?

-To what extent the relativistic electrons of outer belt are influenced by solar wind and IMF?

-What is the contribution of solar protons penetrating to magnetosphere to the trapped population (radiation belts)? Which are the control processes in interplanetary space influencing penetration of solar CR into magnetosphere?

-***Preparing the forecasts for measurements in future experiments with CR (AMS 02) with use of simulations and theoretically known principles of modulation (p, e, …). What will be its consistence with measurements.***

Activities of Department of Space Physics IEP SAS Košice at http://space.saske.sk.

Review “On energetic particles in space” at

http://www.physics.sk/aps/pubs/2009/aps-09-05/aps-09-05.pdf

In 04/2009 there was created in East Slovakia „Center of Space Studies: influences of space weather“, Astronomical Institute SAS T. Lomnica, partners IEP SAS Košice and U. P.J. Šafárik in Košice (Structural Funds of EU).

This presentation was created by the realisation of the project ITMS No. 26220120009, based on the supporting operational Research and development program financed from the European Regional Development Fund.